博　士　論　文

Estimating spectral information of Reflection, Cameras and Illumination

(物体反射・画像センサ・光源の分光情報推定に関する研究)

東京大学大学院
情報理工学系研究科
電子情報学専攻

48-097403　　韓　帥

指導教員　　佐藤 洋一　教授

平成23年12月

Abstract

Appearance of objects in captured images and videos not only relies on objects themselves, but also significantly depends on imaging sensors and illuminations. Therefore, investigating how light emitted from light source interacts with objects and sensors has been an important task for a variety of applications in computer vision field. It is well known that light spans in a wide wavelength range, thus this interaction should be analyzed in spectral domain. However, it is hard to carry out the analysis because dominating equipments usually provide RGB 3 values only which are far from enough for spectral information estimation in the visible wavelength range. To deal with this problem, we present a framework for estimating spectral information of objects, cameras and illumination in this thesis.

First, we show a system to recover spectral reflectance of objects with high temporal resolution. Spectral reflectance offers intrinsic characteristics of objects that are independent of illuminations and sensors. This direct representation about the objects is useful for solving many computer vision problems. However, existing methods for spectral reflectance recovery are limited either by their low temporal resolution or requirement for special hardware. To remove these limitations, we present a novel system for spectral reflectance recovery by exploiting the unique color-forming mechanism of Digital Light Processing (DLP) projectors. DLP projectors use color wheels which are composed of several color segments and rotate quickly to produce desired light. We make effective use of this mechanism and show that a DLP projector can be used as a light source with spectrally distinct illuminations when we capture scenes' appearance under the projector's irradiation by a high-speed camera. Our imaging system is built

on easily available devices and capable of conducting spectral measurements at 100Hz. Based on the measurements obtained by our system, spectral reflectance of the scene is recovered using a linear approximation of surface reflectance. We carefully evaluate the accuracy of our system and demonstrate its effectiveness by spectral relighting of dynamic scenes with fast-moving objects.

Then, we use fluorescence to estimate camera spectral sensitivity under unknown illuminations. Camera spectral sensitivity is an indispensable factor for various color-based computer vision tasks. Though several methods have been proposed to estimate it, their applications are all severely restricted by the requirement for a known illumination spectrum. In this thesis, we present a single-image estimation method using fluorescence with no requirement for a known illumination spectrum. Under different illuminations, the spectral distributions of fluorescence emitted from the same material remain unchanged up to a certain scale. Thus, a camera's response to the fluorescence would have the same chromaticity. Making use of this chromaticity invariance, the camera spectral sensitivity can be estimated under an arbitrary illumination whose spectrum is unknown. Through extensive experiments, we proved that our method is accurate under different illuminations.

Finally, based on the estimated camera spectral sensitivity, we show how to recover spectra of daylights with high accuracy. Making use the estimated camera spectral sensitivities and daylight spectra, color correction problems can be solved. Results show that images after the correction match the target images well.

Acknowledgements

I could never have completed this work without the support and assistance of many people. First and foremost, I would like to express deepest gratitude to my advisor, Prof. Yoichi Sato, for his excellent guidance, valuable suggestions, and kind encouragement in academic. With his help, I learned how to define research problems and formalize them; how to design solutions and improve them; and how to write papers and present them. I also would like to thank Prof. Imari Sato from National Institute of Informatics (NII), Prof. Takahiro Okabe from University of Tokyo and Dr. Yasuyuki Matsushita from Microsoft Research Asia. Their insight and passion for the research teaches me how to face and overcome difficulties and setbacks, and helps me grow as a researcher with a positive and optimistic view of life. For their consistent and generous support, I thank them from the bottom of my heart.

I also would like to express grateful thank to all members of Sato Laboratory, especially to Dr. Yusuke Sugano, Dr. Daisuke Sugimura, and Dr. Michihiro Kobayashi for their kind advices, helpful assistance, technical support and countless hours of useful discussion on the direction and many issues regarding to my research and life. I would like to thank the secretaries, Sakie Suzuki, Yoko Imagawa, Chio Usui for their support and kindness. I would appreciate the final defense committee members: Prof. Kiyoharu Aizawa, Prof. Takeshi Naemura, Prof. Nobuaki Minematsu, Prof. Shunsuke Kamijo

and Prof. Masashi Toyoda, for their valuable comments and suggestions to my work.

This thesis would not have been possible without generous financial support from Japanese Government (Monbukagakusho) Scholarship program. Through its very kind staffs, Monbukagakusho also provides students accommodation and other convenient life supports. These supports are gratefully acknowledged.

I also would like to thank my friends. Without them, my life in Japan will not be so happy and harmonious.

Finally, all this would have not been worthwhile, but for my family. It is impossible to put into words my feelings of loves and gratitude for my parents. It is their understanding, perpetual support, and unconditional love that make me overcome all the difficulties through all the years of my study in Japan.

December 2011

Contents

List of Figures

List of Tables

Chapter 1

Introduction

To a lot of vision tasks, such as image based 3D modeling, tracking, object recognition *etc*, objects' appearance is the basic input. To acquire objects ' appearance, the fundamental approach is using cameras to take images or videos. However, in captured images or videos, objects' appearance not only relies on objects themselves, but also relates to illumination and sensors. Sometimes, the appearance variation caused by different illuminations or different sensors would result in failure of existing methods. So, exploring how illumination, objects and sensors interact with each other in imaging process has become a basic problem for a wide range of research fields, *e.g.* computer vision, computer graphics and digital image processing.

1.1 Motivations

Light is electromagnetic radiation that has a wide wavelength range. Its spectral distribution is known as illumination spectrum. When light emitted from light sources reaches objects' surface, a portion will get reflected. To light with different wavelength, different portion will get reflected, this

is called spectral reflectance of objects, a property determined by objects themselves. If reflected light is perceived by cameras, it will be transformed into RGB or gray-scale values. The relationship between light with different wavelength and the different output is termed as camera spectral sensitivity, a property of sensors. From above discussion, we know that, objects, camera and illumination interact with each other in spectral domain. Therefore, their properties and the interaction among them should be modeled and analyzed in spectral domain. However, it is not easy to get their spectral information based on off-the-shelf components. Not only because the required equipments for spectral measurement, like spectrometer, are expensive; but also due to the fact that measurement is hard to be conducted for the laborious calibration and the time-consuming process. To make the estimation convenient and more practical, several methods are proposed in this work. We hope these methods will offer researchers an easier and more practical approach for estimating spectral information of objects, cameras and illumination.

1.2 Overview

Objects, camera and illumination are 3 independent factors. Therefore, we intuitively divide our task into three sub-tasks in this thesis: (1) Recovering spectral reflectance of objects; (2) Estimating spectral sensitivity of cameras; (3) Estimating spectrum of illumination. The overview of this thesis is given as follows:

1.2.1 Recovering spectral reflectance of objects in dynamic scene.

Spectral reflectance offers intrinsic characteristics of objects that is independent of illuminations and imaging sensors. This direct representation about objects is useful for solving many computer vision problems, like color constancy, material discrimination and relighting. For recovering spectral reflectance, most existing methods focus on static scene. Recently, how to do this recovery for dynamic scene has attracted more and more attentions. Several methods are proposed. But, these works require specially designed hardware, *e.g.* LED clusters, which makes their systems hard to be duplicated by other users. To deal with this problem, we present a novel system for spectral reflectance recovery with high temporal resolution by using Digital light processing (DLP) projectors. DLP projectors use color wheels to produce colors. For color wheels rotate at high rates, light emitted from DLP projectors varies rapidly. Using high-speed cameras to capture scenes' appearance under a projector's irradiation, the DLP projector can be seen as a light source with spectrally distinct illuminations. Representing spectral reflectance with a linear model, spectral reflectance of scene points can be estimated by their appearance under these distinct illuminations. The advantage of our imaging system is that: (1) The whole system is built on easily available devices, no self-made components is used. A similar system can be built easily. (2) Using DLP projectors, working space is comparatively big, calibration is simple. (3)Our system is capable of conducting spectral measurements at 100Hz, which is the fastest system as far as we are concerned. It can be used to measure scene with fast moving objects.

1.2.2 Estimating camera spectral sensitivity without knowing illumination spectrum.

Camera spectral sensitivity is the connection between perceived light and output values of cameras, which plays an indispensable rule to a lot of color-based applications, such as color constancy and multispectral imaging. To estimate camera spectral sensitivity, former works need to know spectral distributions of illumination, which can be measured by spectrometer only. This requirement greatly limits the applicability of existing methods. In this thesis, we use fluorescence instead of reflectance to remove the requirement for illumination spectrum. Under different illuminations, spectral distributions of fluorescence emitted from the same fluorescent material have the same shape but different scales. So the response of a camera to the fluorescence would have the same chromaticity but different intensities. Using this chromaticity invariance of fluorescence, we propose a single-image method to estimate camera spectral sensitivity without knowing illumination spectrum, by which the practicability can be significantly improved. For fluorescence, a calibration board is built by smearing different fluorescent paint on a black board. Through calibration, their spectral reflectance and emission spectra are acquired. Expressing camera spectral sensitivities with a limited number of Fourier basis functions, sensitivity of camera can be estimated by the fluorescent components of the calibration board. Through estimating spectral sensitivities of different cameras under different illuminations whose spectral distributions are unknown, the robustness and the accuracy of our method have been demonstrated.

1.2.3 Estimating spectrum of daylight reusing the image for camera spectral sensitivity estimation.

Daylight is the combination of all direct and indirect sunlight during the daytime. For a big portion of images are captured under daylight conditions, knowing spectrum of daylight would be very helpful to outdoor imaging. In this thesis, we are capable of estimating spectrum of daylight just by the same image captured for camera spectral sensitivity estimation. This means that, by only one image, we are able to estimate not only camera spectral sensitivity, but also daylight spectrum. Through experiments, it can be learned that estimated results match the ground truth very well. Next, we apply estimated camera spectral sensitivities and daylight spectra to color correction problems. After color correction, difference between images about the same scene but under different daylights or captured by different cameras can be reduced significantly. Here, we limit the estimated illumination to daylight due to the fact that: dimensionality of illumination is much higher than reflectance, it is impossible to do the estimation through reflection. On the other hand, daylight can be well approximated by 3 bases. So, in this work, we estimate daylight only.

Chapter 2

Estimating spectral reflectance of objects in dynamic scene

2.1 Background

The amount of light reflected on an object's surface varies for different wavelengths. The ratio of spectral intensity of reflected light to incident light is known as the spectral reflectance. It is an intrinsic characteristic of objects that is independent of illuminations and imaging sensors. Therefore, spectral reflectance offers direct descriptions about objects that are useful to computer vision tasks, such as color constancy [Fin95], material discrimination [SH99], relighting [AACP99] *etc.*

Several methods have been proposed for spectral reflectance recovery. Maloney used an RGB camera to recover the spectral reflectance under ambient illumination [MW86]. This method is limited by its low recovery accuracy due to its RGB 3-channel measurements. To get measurements that contain more than 3 channels, some works attach filters to a light source to modulate the illumination [CHM10] or sequentially place a set of band-pass

filters in front of a monochromatic camera to produce a multi-channel camera [Tom96]. Since switching among filters is time-consuming, these methods are unsuitable for dynamic scenes. To increase temporal resolution, specially designed clusters of different types of LEDs were created [PLGN07]. The LED clusters work synchronously with an RGB camera for conducting spectral measurements at 30 fps. Since such self-made light sources, as well as the controller for synchronization, are not easily available, a level of effort is required to build a similar system.

What we seek is a practical system for fast spectral reflectance recovery built on easily available devices. In this thesis, we exploit the unique color-forming mechanism of Digital Light Processing (DLP) projectors and apply it for spectral measurements. DLP projectors use color wheels to produce the desired light. The color wheels are composed of several specially designed color segments, and light that gets through these segments has specific spectral distributions. In other words, DLP projectors are capable of providing several spectrally distinct illuminations. When the color wheels rotate, the light emitted from the DLP projectors rapidly switches among these illuminations. Making use of this temporal switch of illumination, we built an imaging system that takes spectral measurements with a high temporal resolution.

In the system, a DLP projector is used as a light source, and a high-speed camera is used to capture the scenes' appearance under the projector's irradiation. In order to reduce the number of required measurements for an accurate spectral reflectance recovery, we represent the spectral reflectance as a linear combination of a limited number of spectral bases, which was done in previous studies [J.C64, PHJ89]. Using this linear model, the spectral reflectance of the scene points can be reconstructed by using every five

consecutively captured frames.

Our contributions are summarized below.

- **Dense temporal spectral measurement:** Our system is capable of taking spectral measurements at 100 Hz. This enables measurement for the fast-moving objects, and the recovered results are degraded little by motion artifacts.

- **Easily built imaging system:** Considering that high-speed cameras are becoming readily available in end-user markets, and our system does not require synchronization between the projector and the camera, a similar system can be easily replicated by others. Furthermore, using a DLP projector as a light source, the irradiation uniformity within the entire projection plane can be guaranteed, so the calibrations are simple and the working volume is large.

This chapter is organized as follows. Section 2.2 gives a brief review of the related works about spectral reflectance recovery and DLP-based active vision. Section 2.3 presents our imaging system and its use for spectral reflectance recovery. Section 2.4 verifies its spectral accuracy and temporal accuracy by Macbeth ColorChecker. Section 2.5 shows the relighting results of static and dynamic scenes. We conclude this chapter in Section 2.6.

2.2 Related works

2.2.1 Spectral reflectance recovery under passive illumination

Spectral reflectance can be recovered under passive illumination. Maloney and Wandell used color constancy for spectral reflectance recovery in a scene

with incomplete knowledge of ambient light[MW86]. When using an RGB 3-channel camera as the sensor, surface reflectance had only 2 degrees of freedom which severely limits the accuracy of this method. For accurate results, Tominaga put a set of band-pass filters in front of a monochromatic camera to get measurements more than 3 channels[Tom96]. Because different filters allow light in different wavelength range to get through, Intensities of reflected light in those ranges can be represented by captured images. However, high spectral accuracy requires a large set of filters, and these filters need to be exchanged one by one. The trade-off for accurate spectral resolution is the low temporal resolution. Thus, this method is unsuitable for dynamic scenes.

2.2.2 Spectral reflectance recovery by active illumination

Other existing methods for spectral reflectance recovery rely on active illumination. DiCalro and Wandell recovered the spectral reflectance as an intermediate result [DXW00]. In their work, flash and no-flash image pairs were captured by an RGB camera. Using these image pairs, the authors computed flash-only images, and used them to estimate the spectral reflectance. Because the flash-only images have 3 measurements only (RGB), spectral reflectance was expressed as a combination of three spectral bases. Therefore, like Ref. [MW86], the accuracy of recovered reflectance is limited. To recover spectral reflectance with high accuracy, D'Zmura proposed a method using distinct illuminations[D'Z92], but the author only showed the results using synthetic data, and how well the proposed method works for real scenes was left unknown. Cui et al. proposed an algorithm for selecting an optimized set of wide-band filters, and built a multi-illumination system[CHM10]. They at-

tached the selected filters to a light source, and used it as an additional light source for spectral reflectance recovery under ambient illumination. This method works well for static scenes. But, switching among different illuminations is time-consuming, so the system is not applicable for moving objects.

To measure the dynamic scenes, Park et al. built an imaging system based on multiplexed illumination [PLGN07]. They focused on the combinations of different LEDs and built LED clusters to capture 30 fps multi-spectral videos. However, their system requires specially built LED clusters and synchronization between the LED clusters and a camera. Accordingly, their system is not easily available. Moreover, using these self-made LED clusters, irradiation uniformity can be guaranteed only in a small area, so the working volume is quite limited.

2.2.3 Multispectral imaging

Multispectral imaging is a technique which is widely used in remote sensing [Jas96] to retrieve spectral information of reflected light. If the spectral distribution of incident light is known, spectral reflectance can be calculated easily. Therefore, it is a research field which is different but closely related to our work. For multispectral imaging has attracted researchers attention more than a half century, a lot of works are published. Among these works, some measure spectra of scene points directly by trading off temporal resolution [Gat00b, YHF+06b, RJ99, HRMT94, ROGW98, HOH+94, MRT08]; some trade off spatial resolution [KN07, HFHG+05, WLP04, LPL+05, WFHH05]; some use computed tomography [DD95, VMHD07, TOY93, DVD+97, JMMB97, WRJB06, HDS06, HD08]; some employ coded aperture images [BG06, GOL49, SBMS93, HVJ00, MEGS07, AWB08, AAWB09].

Multispectral imaging systems can be built by using filters [YHF06a],

tunable filter [Gat00a] or spatially varying filter [SN02]. The low temporal resolution of these filter-based systems limits their application for dynamic scenes. For multispectral imaging at video rate, Du et al put a triangular prism in front of a monochromatic camera to disperse light into constitute spectra [DTCL09]. However, this system is limited by its low SNR because a occlusion mask has been used, and a tradeoff between spatial resolution and spectral resolution is inevitable.

2.2.4 Active vision using DLP projector

In computer vision field, many works have been done by making use of DLP projector. Nayar et al. implemented a programmable imaging system using a modified DLP projector-camera pair [NBB06]. Users can control the radiometric and geometric characteristics of the captured images by this system. Narasimhan et al. exploited the temporal dithering of DLP projectors for a wide range of applications, such as high frequency structured light, photometric stereo and so on[NKY08]. Zhang and Huang used the fast illumination variation caused by the collaboration between the DMD and the color wheel of a DLP projector for real-time 3D shape measurements [ZH04]. All these three works removed color wheels, and utilized the fast alternation between the "on" and "off" statuses of the digital micromirror device in DLP projectors; the spectral information was disregarded. In contrast, we use the spectral information from the emitted light for the spectral reflectance recovery. Our work is the first to recover spectral reflectance using a DLP projector.

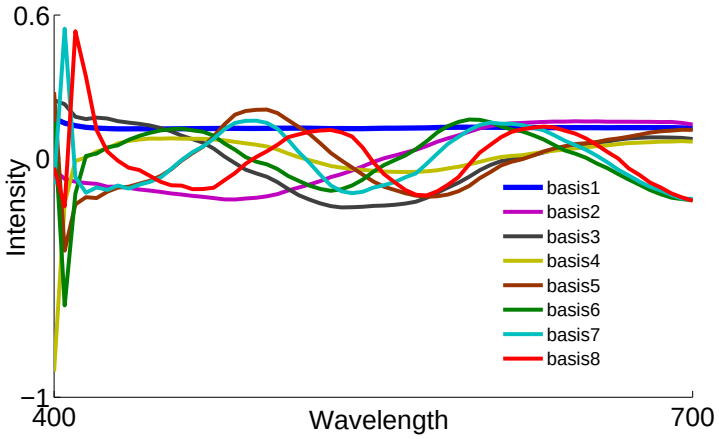

Figure 2.1: 8 bases for spectral reflectance

2.3 Spectral Reflectance Recovery

2.3.1 Three steps for spectral reflectance recovery

There are three factors related to captured image: the incident light, the scene, and the camera. Suppose the camera has a linear intensity response, this relationship can be expressed as

$$I_{m,n} = \int s(\lambda) c_m(\lambda) l_n(\lambda) d\lambda, \tag{2.1}$$

where λ is the wavelength, $I_{m,n}$ is the intensity of a scene point in a captured frame, $s(\lambda)$ is the spectral reflectance of that point, $c_m(\lambda)$ is the spectral sensitivity of the camera at the mth color channel, and $l_n(\lambda)$ is the spectrum of the nth illumination.

The goal of this chapter is to recover spectral reflectance $s(\lambda)$ in a visible range (400−−700[nm]). From Eq. (2.1), we can see that a large set of spectrally distinct measurements are required if we want to recover $s(\lambda)$ with high spectral resolution. To reduce the number of required measurements without

sacrificing spectral resolution, we approximate the spectral reflectance as a combination of a limited number spectral basis functions. This approximation procedure was also used in former works [PLGN07, DXW00].

Several linear models [J.C64, PHJ89] and a nonlinear model [DXW03] have been built by using principal component analysis [TB06] or other tools (see Ref. [KPJ06] for a review about surface reflectance approximation). With regard to how many bases are required for accurate reconstruction, different works have different conclusions [J.C64, PHJ89, Dan92, CCO00, Mal86]. We adopt an 8-dimension linear model for spectral reflectance derived from Ref. [PHJ89] on account of its high reconstruction accuracy. On the basis of this linear model, the spectral reflectance is represented as

$$s(\lambda) = \sum_{j=1}^{8} \alpha_j b_j(\lambda), \tag{2.2}$$

where $b_j(\lambda)(j = 1, 2, .., 8)$ is the jth spectral basis from Ref. [PHJ89] (spectral resolution:10nm) which is show in Fig. 2.1, α_j is the corresponding coefficient. These 8 bases are computed through K-L transformation on the basis of spectral reflectance of 1257 Munsell color chips. Substituting Eq. (2.2) for Eq. (2.1), we obtain

$$I_{m,n} = \sum_{j=1}^{8} \alpha_j \int b_j(\lambda) c_m(\lambda) l_n(\lambda) d\lambda \tag{2.3}$$

Here, we first estimate α_j from observed $I_{m,n}$. Then, spectral reflectance $s(\lambda)$ is reconstructed by substituting α_j into Eq. (2.2).

As shown in Fig. 2.2, our imaging system is composed of a one-chip DLP projector, a high-speed RGB camera with a linear intensity response and a standard diffuse white board which is optional. Using this system, we do spectral reflectance recovery in the follow three steps.

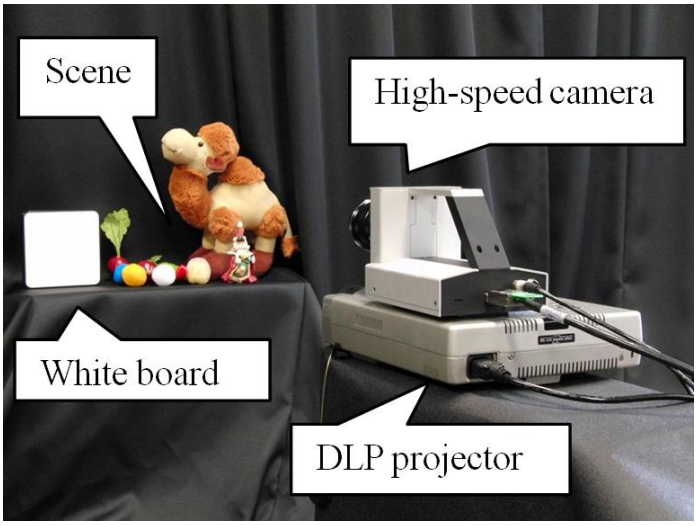

Figure 2.2: Prototype System. Composed of a DLP projector (PLUS^{TM}U2-1130), a high-speed camera (PointGrey^{TM} Lightning) and a white board (labsphere^{TM} SRT-99).

1. Image acquisition: Scene's appearance under the projector's irradiation $I_{m,n}$, is acquired by using the high-speed camera. Every five consecutive frames are used as one measurement for the spectral reflectance recovery. (Section 2.3.2)

2. Illumination recovery: Illumination spectra, $l_n(\lambda)$, changes from frame to frame. To recover the illumination of captured frames, we proposed two methods: one uses the white board as a calibration target; the other one uses captured image sequence. (Section 2.3.3)

3. Spectral reflectance reconstruction: Based on the 8-dimensional linear model, spectral reflectance $s(\lambda)$, can be reconstructed from the acquired images and recovered illumination. (Section 2.3.4)

In the following parts, we explain each of these steps in detail.

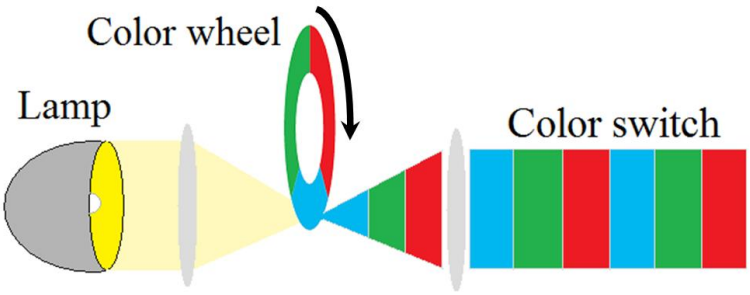

Figure 2.3: Color switch caused by rotation of color wheel. In our system, the DLP projector is equipped with a RGB 3-segment color wheel, thus color verifies among RGB 3 kinds of light temporally.

2.3.2 Image acquisition by color switch

Different from other kinds of projectors, DLP projectors use color wheels to produce the desired light. The color wheel consists of several color segments, and these segments only allow light in a specific wavelength range to get through. When the color wheel quickly rotates, the light emitted from DLP projectors changes rapidly. In our work, this temporal variation in light is referred to as "color switch". A diagrammatic sketch is shown in Fig. 2.3. In our system, a DLP projector equipped with a 3-segment color wheel has been used (PLUS^{TM}U2-1130). since the color wheel rotates at 120 rps (revolution per second), color switch occurs at 360 Hz (3×120).

The human eyes, and common video cameras work at low rates ($24--30$ [Hz]), and thus they cannot detect the color switch. Here, a 500 fps camera (PointGrey^{TM} Lightning) is adopted to take images of scenes under the projector's irradiation. The camera outputs 24bit (8×3) color images at a SXGA resolution (1280×1024). For camera's intensity response, we adjust shutter speed of the camera, corresponding response in RGB 3 channels are plot in Fig. 2.4. We can see that our high speed camera has linear intensity response and in and shift caused by dark current exist. In addition,

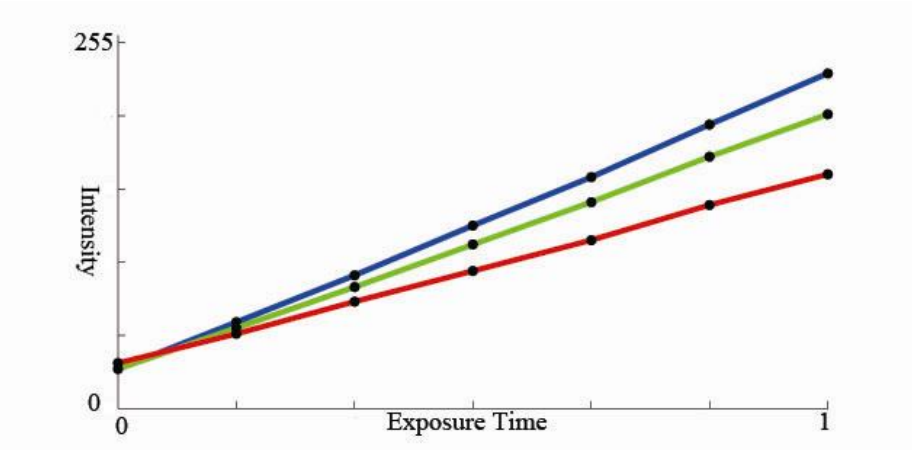

Figure 2.4: Through adjusting camera's shutter speed, its linear intensity response in RGB 3 channels can be verified.

the spectral sensitivity of the camera $c_m(\lambda)$ $(m = 1, 2, 3)$, was measured by using a monochromator and a spectrometer. The monochromator is used to generate a sequence of narrow-band lights. The spectral radiance of these lights is measured by the spectrometer. We expose the camera's sensor to the narrow-band lights and capture images. The relationship between the RGB values in the captured images and the spectral radiance of the corresponding lights, *i.e.*, spectral sensitivity, is shown in Fig. 2.5. During one rotation of the color wheel, the high-speed camera can capture 4.17 frames. So, we use five consecutive frames as one measurement for the spectral reflectance recovery. Fig. 2.6 shows one measurement about Macbeth ColorChecker. We can see that the scene's appearance clearly changes under the color switch of the DLP projector. It should be noted that the color switch occurs at 360Hz, but the camera operates at 500 fps, so the projector and the camera work asynchronously.

2.3.3 Illumination recovery

To keep our system simple, we do not synchronize the projector and the camera. Due to the asynchronism, the illumination changes from frame to

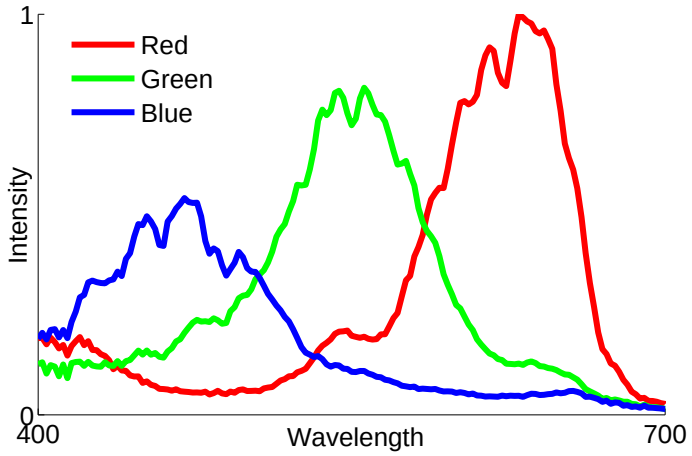

Figure 2.5: Camera's spectral sensitivity for RGB 3 channels which is pre-calibrated by a monochromator and a spectrometer.

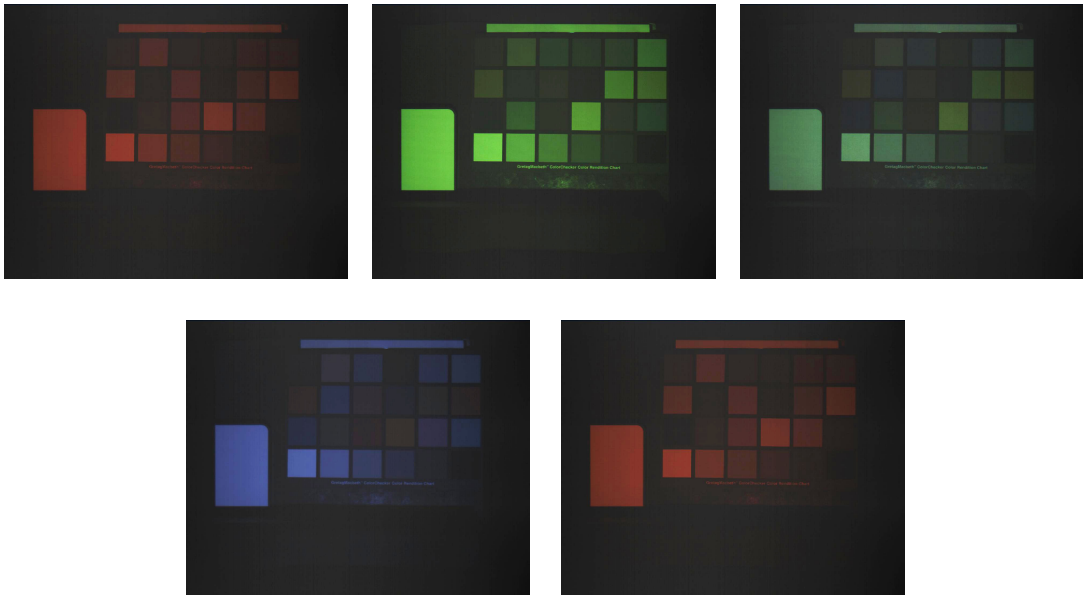

Figure 2.6: One measurement of Macbeth ColorChecker which contains 5 frames captured sequentially by the 500 fps camera in 1/100s. Appearance variation of the ColorChecker under colorswitch can be observed

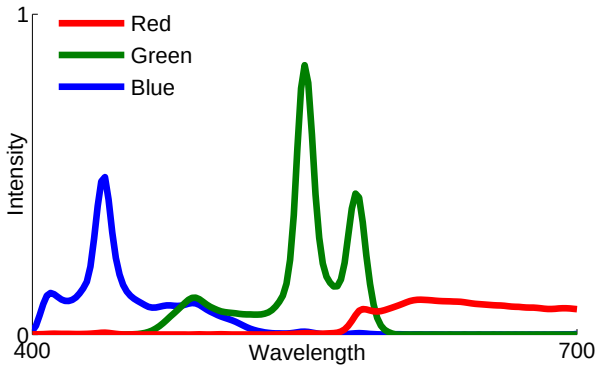

Figure 2.7: Spectra of three distinct illuminations of the DLP projector. These measurements are captured by a spectrometer whose shutter speed is fixed to a relatively big number to keep the measurements accurate.

frame. For spectral reflectance recovery, we need to know corresponding illumination for each captured frame. Therefore, we describe how to recover the illumination spectrum $l_n(\lambda)$ of captured frame in this section.

Using a calibration target

As mentioned above, light that gets through different segments on color wheels has distinct spectral distributions. If we use these spectral distributions as the illumination bases, light emitted from the DLP projectors can be expressed by a linear combination of these bases. In our system, since the three segments of the color wheel correspond to the RGB color filters, we can acquire these three distinct illuminations by inputting the projector (255, 0, 0), (0, 255, 0), and (0, 0, 255) respectively. Their spectra, which are measured by a spectrometer, are shown in Fig. 2.7. For each frame, its illumination spectrum, $l_n(\lambda)$, can be represented as

$$l_n(\lambda) = \sum_{k=1}^{3} \beta_{n,k} p_k(\lambda), \text{ subject to } \beta_{n,k} \geq 0, \tag{2.4}$$

where $p_k(\lambda)$ is the spectrum of the kth illumination basis of the DLP projector, $\beta_{n,k}$ is the corresponding coefficient.

We place a standard diffuse white board (labsphere$^{\text{TM}}$ SRT-99) within the scene as a calibration target.By using Eqs.1 and 4, the brightness of a surface point on the white board is

$$I^w_{m,n} = \sum_{k=1}^{3} \beta_{n,k} \int p_k(\lambda) s^w(\lambda) c_m(\lambda) d\lambda, \tag{2.5}$$

where $I^w_{m,n}$ is the intensity of that point, and $s^w(\lambda)$ means its spectral reflectance. Use $P_{k,m}$ to represent the intensity of the point at the mth channel under the kth illumination basis

$$P_{k,m} = \int p_k(\lambda) s^w(\lambda) c_m(\lambda) d\lambda \ (k = 1, 2, 3), \tag{2.6}$$

Eq. (2.5) can be rewritten as

$$I^w_{m,n} = \sum_{k=1}^{3} \beta_{n,k} P_{k,m}, \tag{2.7}$$

$P_{k,m}(k = 1, 2, 3)$ can be measured by using the high-speed camera to capture images of the white board under three distinct illuminations of the projector. We only need to measure them once in advance.

From Eq. (2.7), we see that the intensity of a surface point on the white board under illumination $l_n(\lambda)$ is a linear combination of its intensities under three illumination bases

$$\boldsymbol{I}^w_n = \left[I^w_{1,n} \ I^w_{2,n} \ I^w_{3,n} \right]^T = \boldsymbol{P}^w \boldsymbol{\beta}_n, \tag{2.8}$$

where $\boldsymbol{I}^w_n$ represents the RGB value of a surface point on the white board under the nth illumination, $\boldsymbol{P}^w$ is a 3×3 matrix consists of $P_{k,m}(k = 1, 2, 3, \ m = 1, 2, 3)$, $\boldsymbol{\beta}_n$ is the corresponding 3×1 coefficient vector.

In principle, $\boldsymbol{\beta}_n$ can be calculated by $\boldsymbol{\beta}_n = (\boldsymbol{P}^w)^{-1}\boldsymbol{I}_n^w$ easily. However, due to the noise , $\beta_{n,k}$ $(k = 1, 2, 3)$ may sometimes be negative. This conflicts with the non-negative constraint of Eq. (2.4). Thus, we solve $\boldsymbol{\beta_n}$ as a non-negative least squares problem:

$$\boldsymbol{\beta}_n = \underset{\boldsymbol{\beta}_n}{argmin} \mid \boldsymbol{I}_n^w - \boldsymbol{P}^w\boldsymbol{\beta}_n \mid^2, \quad \text{subject to } \beta_{n,k} \geq 0 \ (k = 1, 2, 3) \tag{2.9}$$

Using calculated $\boldsymbol{\beta_n}$, illumination spectrum $l_n(\lambda)$ can be reconstructed by using Eq. (2.4).

Without using the calibration target

As described above, illumination of captured images can be recovered by using the white board as a calibration target. This method is simple and efficient, but the drawbacks of using the white board are also obvious: (1) a portion of space is occupied; (2) images of the white board under distinct illuminations need to be captured in advance. So, we want to remove the white board from our system, and recover the illumination of captured images by appearance of scenes in captured images. For this goal, we need to establish the relationship between illumination and scenes' appearance.

Observe the captured images which are shown in Fig. 2.6, we can learn that scene's appearance is closely related to corresponding illumination. If we can model the relationship between illumination and scene's appearance, illumination of captured images can be recovered through exploring scene's appearance.

To model this relationship, we need to know how illumination varies among images. So, we used the method introduced above to calculate $\beta_{n,k}$ (k=1,2,3) of 1000 sequentially captured images. Their distribution is plotted in Fig. 2.8. From these plots, we can learn that:

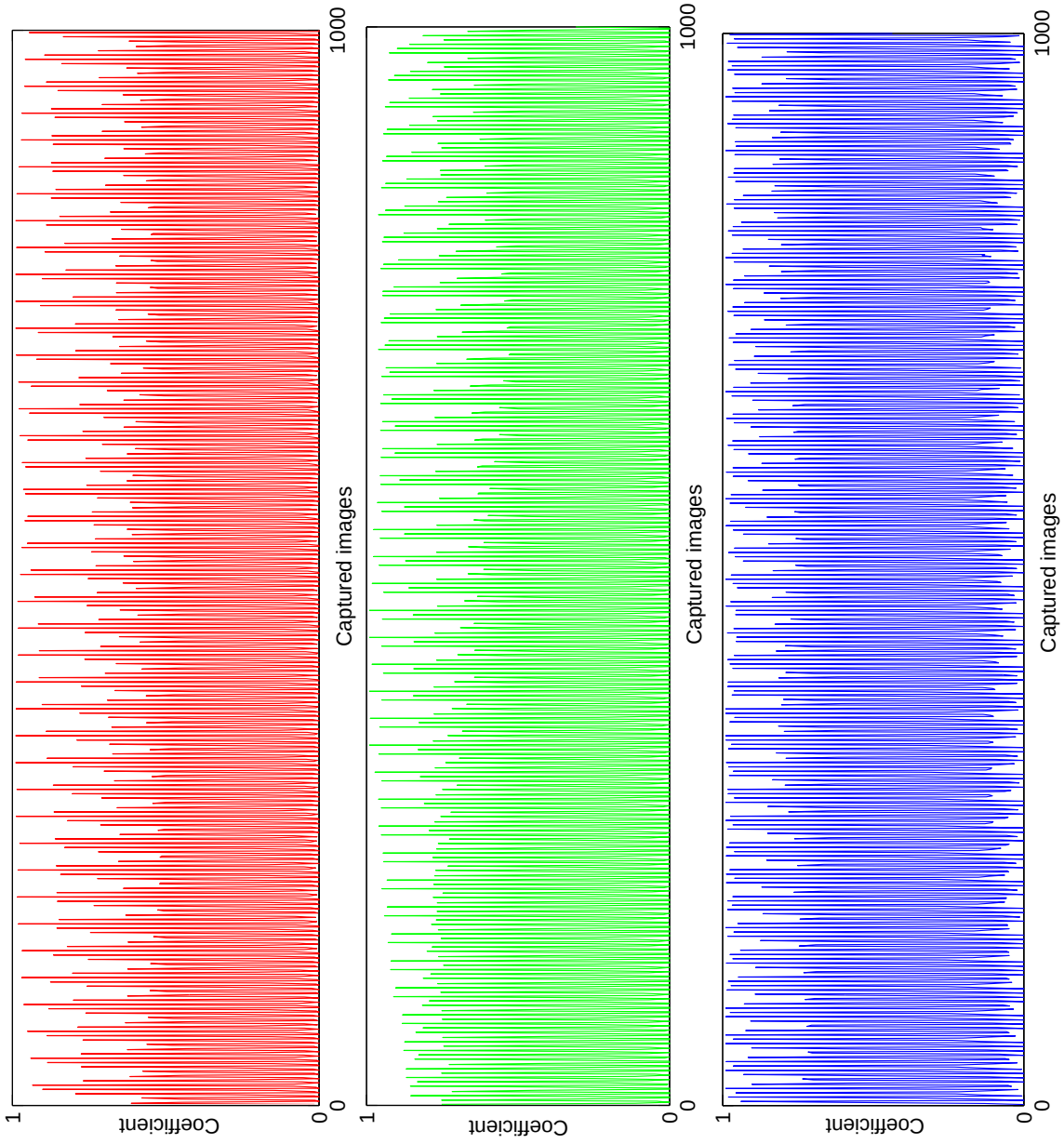

Figure 2.8: Distribution of $\beta_{n,k}$(n=1–3,k=1–1000). Despite the drastically changes in these 3 bands. Peak values of these bands vary little.

.

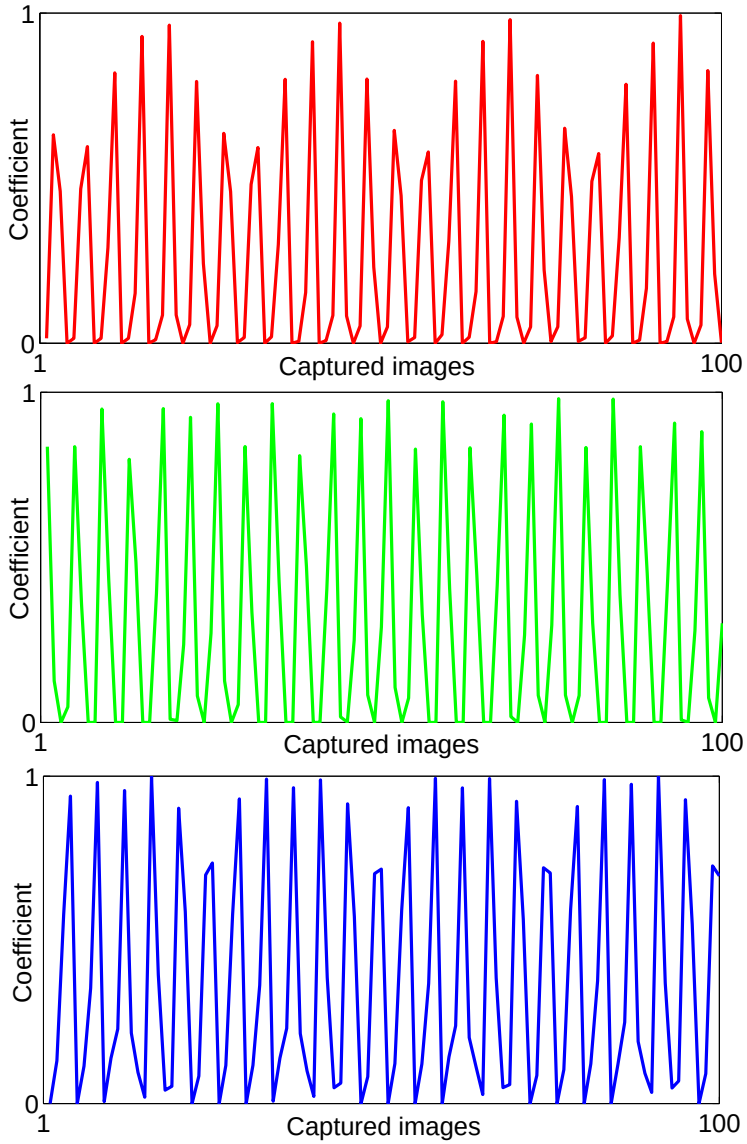

Figure 2.9: Distribution of $\beta_{n,k}$(n=1–3,k=1–100). Peak values of all 3 bands appear as least once in every 25 consecutively captured images.

.

$(X+\frac{0}{500})mode\frac{1}{120}$	$(X+\frac{1}{500})mode\frac{1}{120}$	$(X+\frac{2}{500})mode\frac{1}{120}$	$(X+\frac{3}{500})mode\frac{1}{120}$	$(X+\frac{4}{500})mode\frac{1}{120}$
$X+\frac{0}{3000}$	$X+\frac{6}{3000}$	$X+\frac{12}{3000}$	$X+\frac{18}{3000}$	$X+\frac{24}{3000}$
$(X+\frac{5}{500})mode\frac{1}{120}$	$(X+\frac{6}{500})mode\frac{1}{120}$	$(X+\frac{7}{500})mode\frac{1}{120}$	$(X+\frac{8}{500})mode\frac{1}{120}$	$(X+\frac{9}{500})mode\frac{1}{120}$
$X+\frac{5}{3000}$	$X+\frac{11}{3000}$	$X+\frac{17}{3000}$	$X+\frac{23}{3000}$	$X+\frac{4}{3000}$
$(X+\frac{10}{500})mode\frac{1}{120}$	$(X+\frac{11}{500})mode\frac{1}{120}$	$(X+\frac{12}{500})mode\frac{1}{120}$	$(X+\frac{13}{500})mode\frac{1}{120}$	$(X+\frac{14}{500})mode\frac{1}{120}$
$X+\frac{10}{3000}$	$X+\frac{16}{3000}$	$X+\frac{22}{3000}$	$X+\frac{3}{3000}$	$X+\frac{9}{3000}$
$(X+\frac{15}{500})mode\frac{1}{120}$	$(X+\frac{16}{500})mode\frac{1}{120}$	$(X+\frac{17}{500})mode\frac{1}{120}$	$(X+\frac{18}{500})mode\frac{1}{120}$	$(X+\frac{19}{500})mode\frac{1}{120}$
$X+\frac{15}{3000}$	$X+\frac{21}{3000}$	$X+\frac{2}{3000}$	$X+\frac{8}{3000}$	$X+\frac{14}{3000}$
$(X+\frac{20}{500})mode\frac{1}{120}$	$(X+\frac{21}{500})mode\frac{1}{120}$	$(X+\frac{22}{500})mode\frac{1}{120}$	$(X+\frac{23}{500})mode\frac{1}{120}$	$(X+\frac{24}{500})mode\frac{1}{120}$
$X+\frac{20}{3000}$	$X+\frac{1}{3000}$	$X+\frac{7}{3000}$	$X+\frac{13}{3000}$	$X+\frac{19}{3000}$

Table 2.1: One-to-one correspondence between $(X+\frac{q}{500})mode\frac{1}{120}$(q=0−−24) and $X+\frac{q}{3000}$(q=0−−24).

1. Although all 3 coefficients vary dramatically among these 1000 images, their peak values are almost constant 1.

2. Fig. 2.9 shows β_n (k=1,2,3) of 100 sequentially captured images. The peak values of all 3 coefficients appear at least 4 times in every 100 captured images. In other words, among every 25 consecutively captured images, for each k (k=1,2,3), there are at least one image whose kth coefficient is very close to 1.

The explanation for observation 1 is simple. $\beta_{n,k}$ indicates the share of the kth illumination basis for the nth captured image. Because the high speed camera of our system works at 500fps which is higher than the frequency of colorswitch (360Hz), when illumination for captured images is composed of only 1 illumination basis, their coefficients to that illumination would be 1, the coefficients corresponding to the other illumination bases would be 0.

Observation 2 can be proved. For the DLP projector used in our system

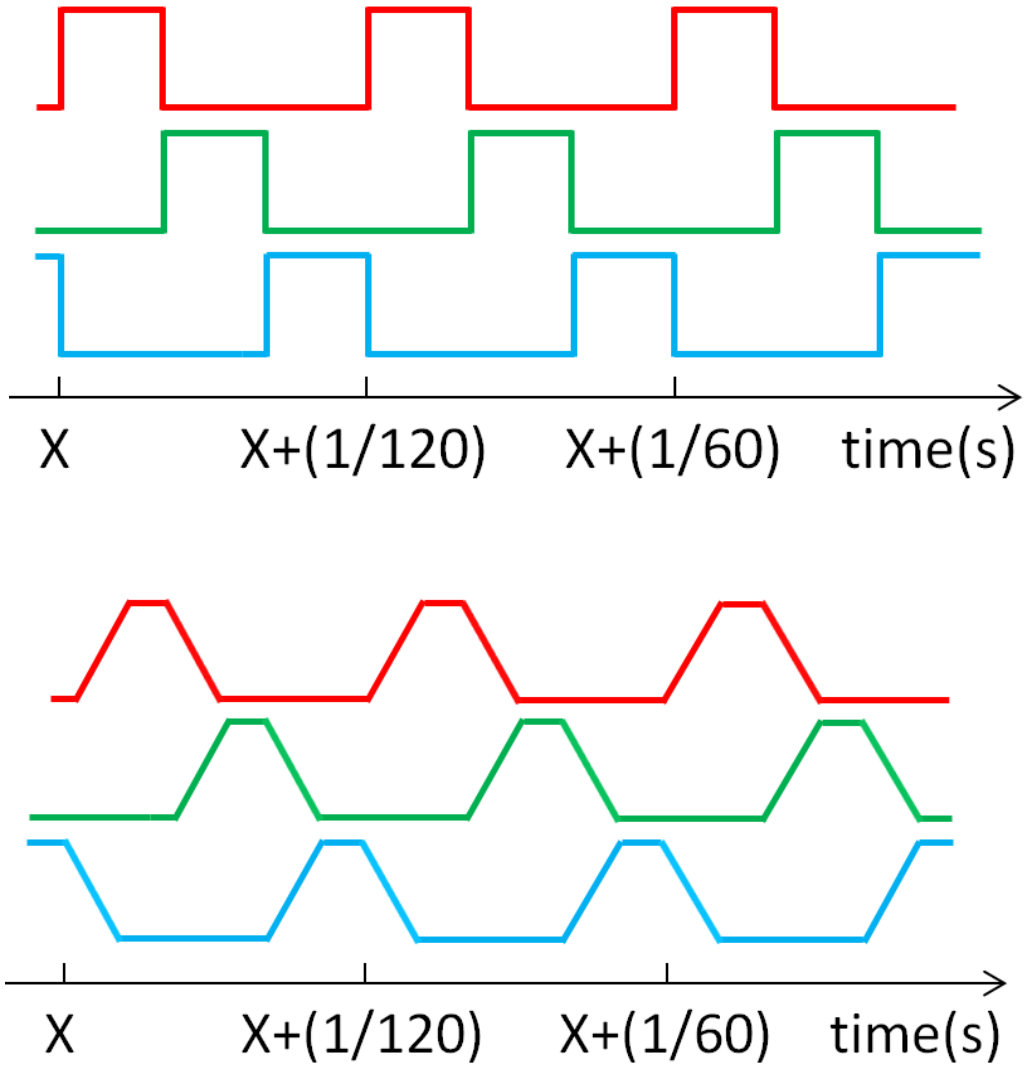

Figure 2.10: Light emitted from DLP projector can be expressed as 120Hz periodic signals (Upper). And, their corresponding integral appears as 120Hz trapezoid signal (Lower).

is equipped with a 3-segment color wheel which rotates at 120 rps, 3 distinct illumination emitted from it can be expressed by 120Hz periodic step signals shown in Fig. 2.10. Our camera works at 500 fps, integral of the periodic step signals during the exposure time of one image, *i.e.*, 1/500s, can be calculated as

$$\beta_{n,k} = \int_{X+\frac{n-1}{500}}^{X+\frac{n}{500}} l_k(t)dt. \tag{2.10}$$

Here, X is used to indicate an arbitrary time point.

$\beta_{n,k}$ $(n = 1, 2, ...)$are discrete samples of continue functions β_k which are shown in Fig. 2.10. It is clear that β_k are also 120Hz periodic signals and appear as isosceles trapezoids. The upper bases of these trapezoids indicate the peak values. β_k of 25 consecutively captured images correspond 25 sampling points with equidistant on the "trapezoid signal", sampling instant is $X + \frac{q}{500}$ (q=0−−24). Since the "trapezoid signal" are 120Hz periodic signals, sampling points at $X + \frac{q}{500}$ and $(X + \frac{q}{500})mode\frac{1}{120}$ have the same value. And, tab. 1 shows that a one-to-one correspondence can be found between $(X + \frac{q}{500})mode\frac{1}{120}$ and $X + \frac{q}{3000}$ (q=0−−24). Thus, the values of 25 sampling points at $X + \frac{q}{500}$ (q=0−−24)can be expressed by the value of 25 points at $X + \frac{q}{3000}$ (q=0−−24). In each period, peak values of the β_k lasts $(\frac{1}{360} - \frac{1}{500})$sec, and $(\frac{1}{360} - \frac{1}{500}) > 2 \times \frac{1}{3000}$, so peak values of β_k would appear at least once in every 25 consecutively captured images.

Superimpose $\beta_{n,k}$ of every 25 consecutively captured images 10 times, results are shown in Fig. 2.11. Clearly, coefficients repeat every 25 images.

To different setup, in which camera does not work at 500 fps or color switch occurs at different rate, the above 2 observations may be not available. It should be analyzed case by case. But, we can confirm one thing: when the camera works 2 times faster than color switch, we can get these 2 observation for sure. This can be explained by Nyquist-Shannon sampling theorem.

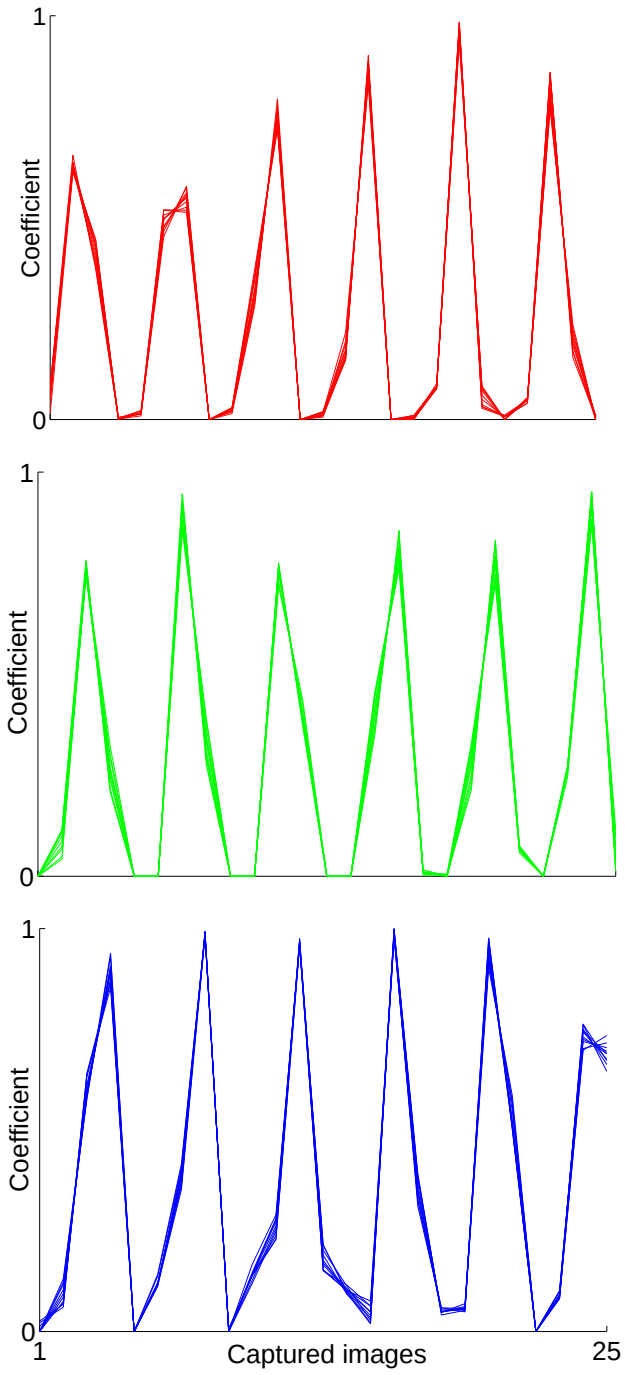

Figure 2.11: Superimpose the coefficients of illuminations of every 25 images, we can see that illumination of captured images repeats in every 25 images

.

Through the analysis above, we can see these 2 observations as 2 properties when using our system. Based on these 2 properties, we will model the relationship between the scene's appearance and the illumination as follow.

Because the camera works at 500 fps, objects can be seen as static in a few consecutively captured images. So, the variation of scene's appearance among these images is caused by the illumination variation. Take the red basis for instance, when a image appears more reddish than the nearby images, its β_1 would be bigger than theirs. If one image is the most reddish one among 25 consecutively captured images, according to property 2, its illumination should be composed of red illumination basis only. Due to property 1, coefficient β_1 equals 1, β_2 and β_3 equal 0, so the spectral distribution of the illumination for that image can be determined.

For the nth captured image, we use $\{R_n, G_n, B_n\}$ to indicate the mean RGB value of all pixels on it. And, the normalized value $\{R_n^{ratio}, G_n^{ratio}, B_n^{ratio}\}$ are calculated to evaluate how reddish, greenish and bluish the image is

$$\{R_n^{ratio}, G_n^{ratio}, B_n^{ratio}\} = \frac{\{R_n, G_n, B_n\}}{R_n + G_n + B_n}. \tag{2.11}$$

For every 25 captured images, we need to select 3 images whose illumination is composed of the RGB illumination basis respectively. Here, we take "red" image to illustrate the procedure which contains two steps.

1. Sort these 25 images based on their R^{ratio}.
2. Among the 6 images whose R^{ratio} is bigger than the others, selected the one whose red value is the biggest as the "red image".

In our system, camera captures 25 images while color wheel rotates 6 round. Pick one image out of 6 in step (2) can help us finding out the real "red" images despite variety kinds of scene. In this way, 1 image is selected from every 25 images. For a sequence containing q images, we would have

as many as $q \ mod \ 25$ images. Considering the variation caused by dynamic scenes, we temporally interpolate the mean RGB values of these "red", images. In this way, the nth(n=1−−q) captured image would corresponds a vector: $\{R_n^{Rmax}, G_n^{Rmax}, B_n^{Rmax}\}$, the interpolated results of the mean RGB values of "red" images.

By the same procedure, "green" and "blue" images also can be selected. After the temporal interpolation, the nth(n=1−−q) captured image would corresponds 3 vectors: $\{R_n^{Rmax}, G_n^{Rmax}, B_n^{Rmax}\}$, $\{R_n^{Gmax}, G_n^{Gmax}, B_n^{Gmax}\}$ and $\{R_n^{Bmax}, G_n^{Bmax}, B_n^{Bmax}\}$

From the discussion above, we know these 3 vector correspond RGB 3 illumination bases. Just like the method used in section 2.3.3, we use the 3×3 matrix formed by these 3 vectors instead of the $\boldsymbol{P}^w$ in Eq. (2.9) to calculate β_n

$$\boldsymbol{\beta}_n = \underset{\boldsymbol{\beta}_n}{argmin} \mid \begin{pmatrix} R_n \\ G_n \\ B_n \end{pmatrix} - \begin{pmatrix} R_n^{Rmax} & R_n^{Gmax} & R_n^{Bmax} \\ G_n^{Rmax} & G_n^{Gmax} & G_n^{Bmax} \\ B_n^{Rmax} & B_n^{Gmax} & B_n^{Bmax} \end{pmatrix} \boldsymbol{\beta}_n \mid^2, \quad \text{subject to } \beta_{\mathrm{n,k}} \geq 0 \ (\mathrm{k} = 1, 2, 3) \tag{2.12}$$

Once we get β_n, illumination for the nth image can be computed. Fig. 2.12 show us the recovered illumination of the 5 images in Fig. 2.6. Through these 2 methods. We can see that the results are similar but different. To evaluate how different the recovered results are, we consecutively capture 100 images of a static Macbeth ColorChecker with a white board placed in the scene. Their illuminations are recovered by the 2 method introduced in this section respectively. For the nth captured image, we use β_n^{WB} and β_n^{MC} to indicate the recovered illumination by the white board and by the appearance of the Macbeth ColorChecker part in the image. Thus, every

image corresponds two 3×1 vectors. The difference between them is defined as $\beta_n^{Diff} = \beta_n^{MC} - \beta_n^{WB}$. β_n^{Diff} is also a 3×1 vector. Distribution of its 3 element, $\beta_{n,k}^{Diff}$ (n=1−−100,k=1−−3), are shown in Fig. 2.13. We can see that for all 3 coefficients, the difference varies in a very narrow band (-0.1, 0.1) which means that recovered results are very similar to each other.

From above discussion, we know that the proposed method for illumination recovery using calibration target is scene-independent. On the contrary, the method without using calibration target relies on the scene, and its accuracy of recovered illumination varies regarding different scenes. This variation is caused by different matrix in Eq. (2.12) which is determined by the scene. For scenes in which objects have flat reflectivity to light in whole visible wavelength range [400−−700nm], like the Macbeth ColorChecker, these two methods would provide the same accuracy of recovered illumination. However, if scenes have low reflectivity in some range of wavelength, condition number of the 3×3 matrix in Eq. (2.12) would be big, calculation of β_n by Eq. (2.12) would be unstable. In such a case, method using calibration target would perform better.

2.3.4 Spectral reflectance reconstruction using constrained model

$l_n(\lambda)$ is recovered in Section 2.3.3. Recall Eq. (2.1), the integral in it can be represented as known coefficients: $f_{j,m,n} = \int b_j(\lambda)c_m(\lambda)l_n(\lambda)d\lambda$. One measurement that contains five consecutive frames can be written in matrix form as

$$\boldsymbol{I} = \boldsymbol{F}\boldsymbol{\alpha}, \tag{2.13}$$

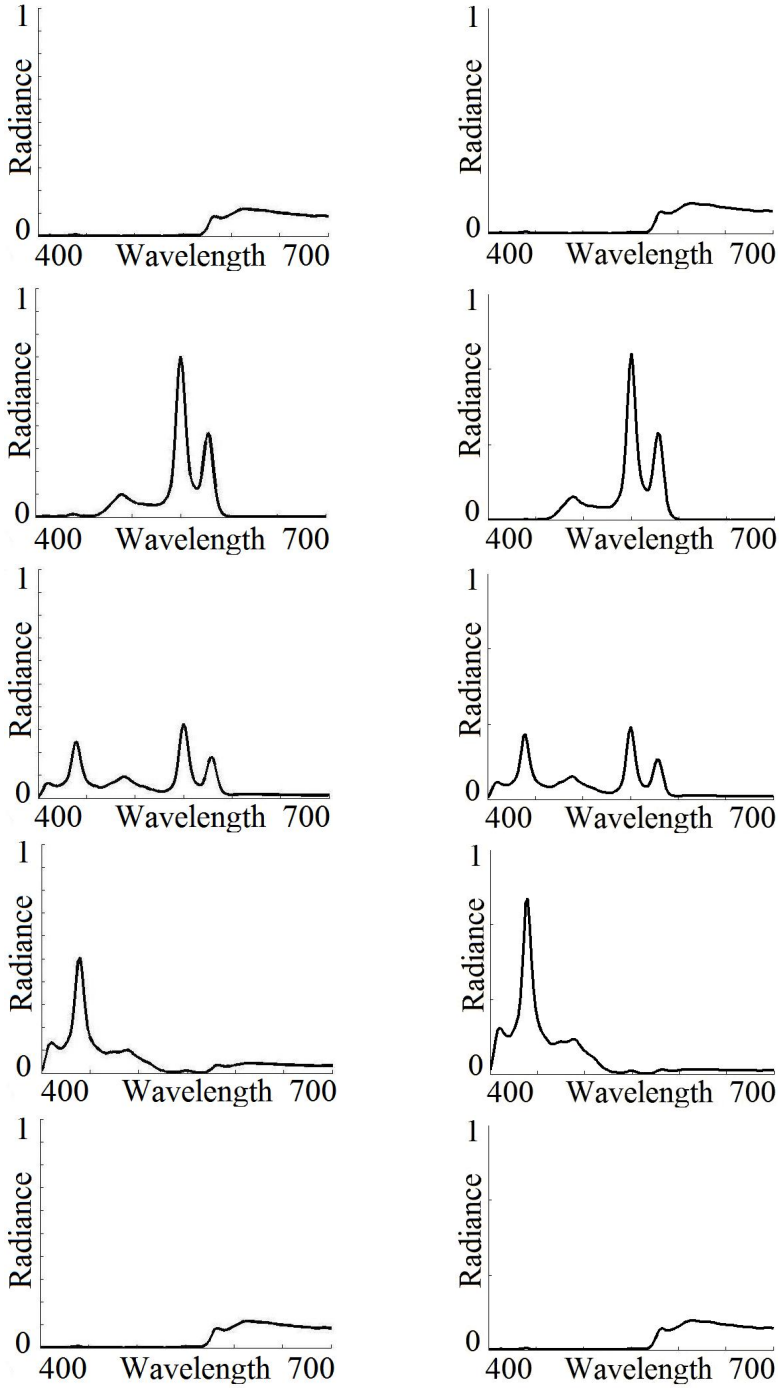

Figure 2.12: Recovered illumination spectra of the 5 images in the measurement of Macbeth ColorChecker shown in Fig. 2.6. Left column: recovered results using calibration target. Right column: recovered results without using calibration target. Compare with these 2 sets, their similarity and difference can be reveled.

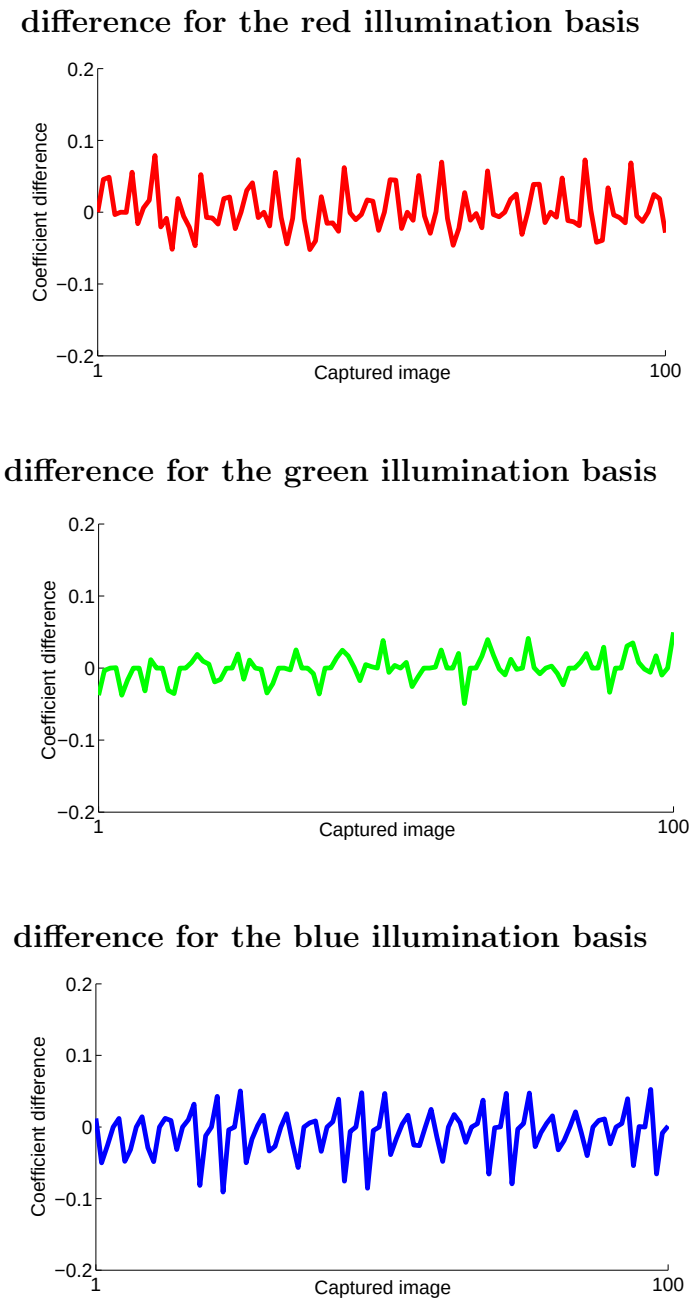

Figure 2.13: Difference between recovered illumination coefficients by using white board and without using white board for 100 consecutively captured images.

where $\boldsymbol{I}$ is a 15×1 vector (15 measurements: RGB 3 channels $\times$ 5 frames), $\boldsymbol{F}$ is a 15×8 matrix (15 measurements $\times$ 8 spectral bases), and $\boldsymbol{\alpha}$ is an 8×1 coefficient vector.

If $\boldsymbol{\alpha}$ is estimated from $\boldsymbol{I}$, spectral reflectance $s(\lambda)$ can be reconstructed by Eq. (2.2). In this way, the problem of spectral reflectance recovery can be solved by the 8 coefficients estimation. The DLP projector in our system has three spectrally distinct illuminations, and the high-speed camera provides a 3-channel measurement under each illumination. In total, we can obtain 3×3, *i.e.*, 9 effective channels. Thus, the problem of estimating 8 coefficients is over-determined. However, using the least squares solution in Eq. (2.13), the reconstructed spectral reflectance does not always satisfy the non-negative constraint and the solutions tend to be unstable. Therefore, we adopted the constrained minimization method proposed in Ref. [PLGN07]. The first derivative of the spectral reflectance respective to λ is used as the constraint:

$$\begin{aligned} \boldsymbol{\alpha} = \underset{\boldsymbol{\alpha}}{argmin} \left[\mid \boldsymbol{I} - \boldsymbol{F}\boldsymbol{\alpha} \mid^2 + \gamma \mid \frac{\partial s(\lambda)}{\partial \lambda} \mid^2 \right], \\ \text{subject to } \mathrm{b}_{\boldsymbol{m}}\boldsymbol{\alpha} \geq 0 \text{ for all } \lambda, \end{aligned} \tag{2.14}$$

where γ is a weight for the constraint term. $\boldsymbol{b_m}$ is a 31×8 matrix whose columns are the 8 spectral bases.

2.4 Accuracy Evaluation

In our system, every five consecutive captured frames by the 500 fps camera are used as one measurement. Thus, the spectral measurements are taken at 100 Hz. However, the color wheel rotates at 120 rps. Due to the asynchronism between the DLP projector and the camera, illumination spectra of the 5 frames which belong to the same measurement change from measurement to

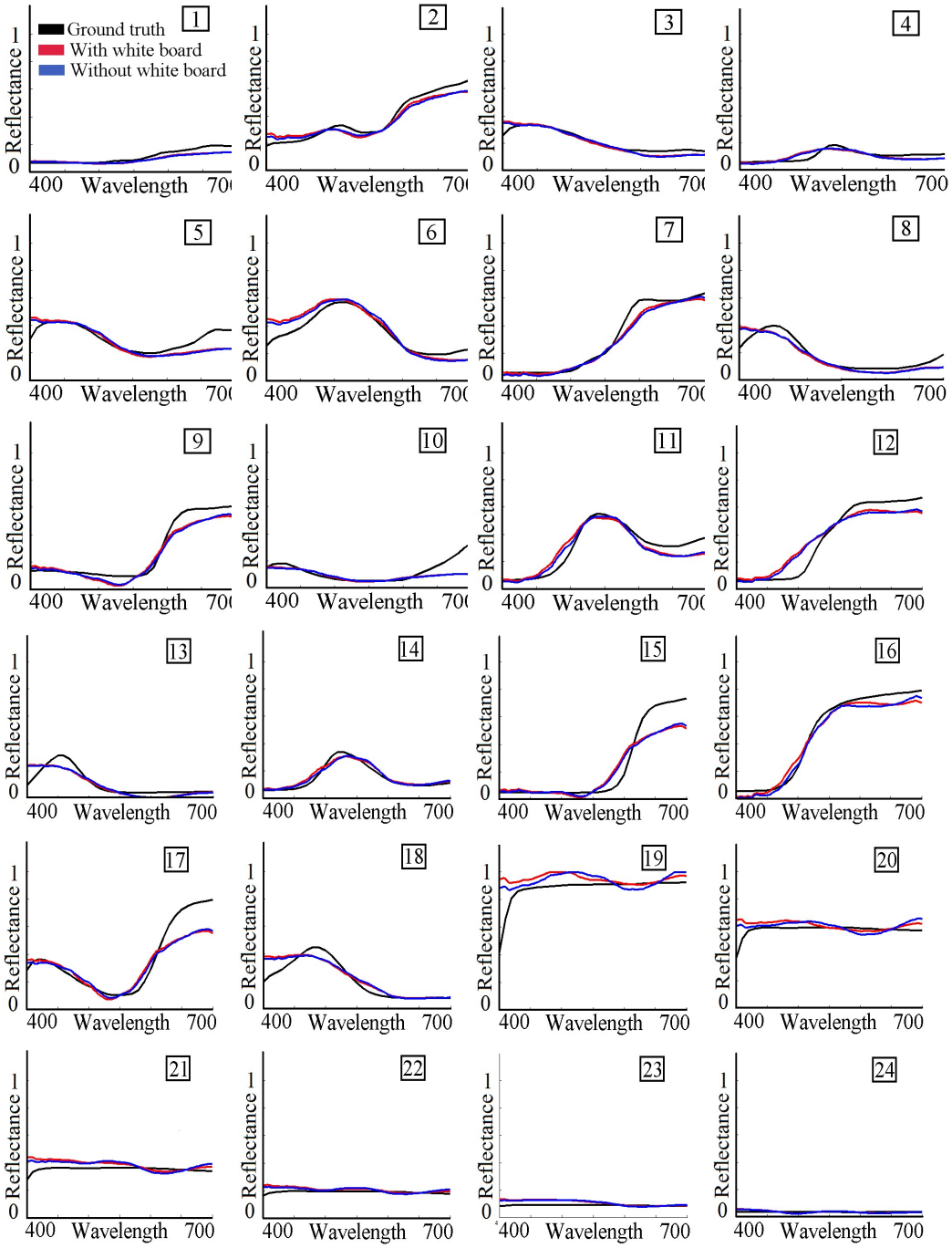

Figure 2.14: Recovered spectral reflectance of all 24 clips on Macbeth ColorChecker by the measurement shown in Fig. 2.6.

measurement. The accuracy of the recovered results would be affected by this temporal illumination variation. Thus, we need to evaluate both the spectral accuracy and temporal accuracy of our system in this section.

Besides, two methods for illumination recovery are proposed in section 2.3.3, so every image corresponds two recovered illumination spectra. And, the results shown in Fig. 2.13 indicate that the difference between them is small but still can not be ignored. Therefore, it is very necessary to explore the accuracy variation caused by this difference. Therefore, for an image set, 4 results need to be revealed: the spectral accuracy and the temporal accuracy, with and without using the white board as calibration target.

Here, we evaluate the accuracy of our system by Macbeth ColorChecker which contains 24 clips. The spectral reflectance of these clips is known. We used 500 consecutively captured images of the static Macbeth ColorChecker as the image set. As stated before, 5 images were used as 1 measurement, so we got 100 measurements. For these 100 measurements, we used the methods stated in section 2.3.3 to recover the illumination spectrum of every image; set γ in Eq. (2.14) to 50 and recovered the spectra reflectance of all 24 clips based on the measurement (Fig. 2.14 shows us the recovered results using the measurement given in Fig. 2.6). In this way, every clip corresponds 100 reconstructed results. The root mean square (RMS) error of these reconstructed results was calculated. The maximum, mean, and minimum among the 100 RMS error values for every clip are also computed, results are shown on the upper side of Fig. 2.15. The lower side of Fig. 2.15 shows us the results of the same image set, but different illumination recovery method which is introduced in section 2.3.3.

In both 2 histograms shown in Fig. 2.15, we can see that the maximum RMS error of recovered spectral reflectance of all 24 clips does not deviate a

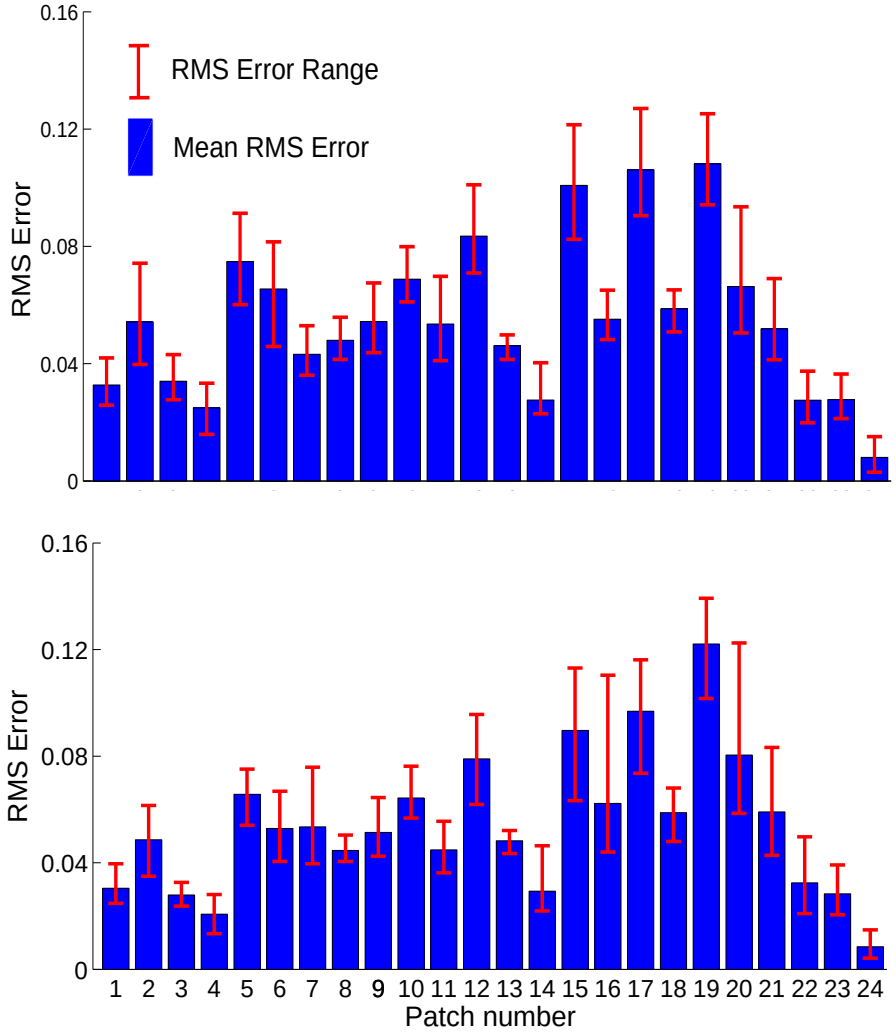

Figure 2.15: Spectral accuracy evaluation. For each clip, blue column indicate corresponding mean RMS error; Red error bar indicates range of errors of 100 measurements. Upper: Spectral accuracy using white board; Lower: Spectral accuracy without using white board.

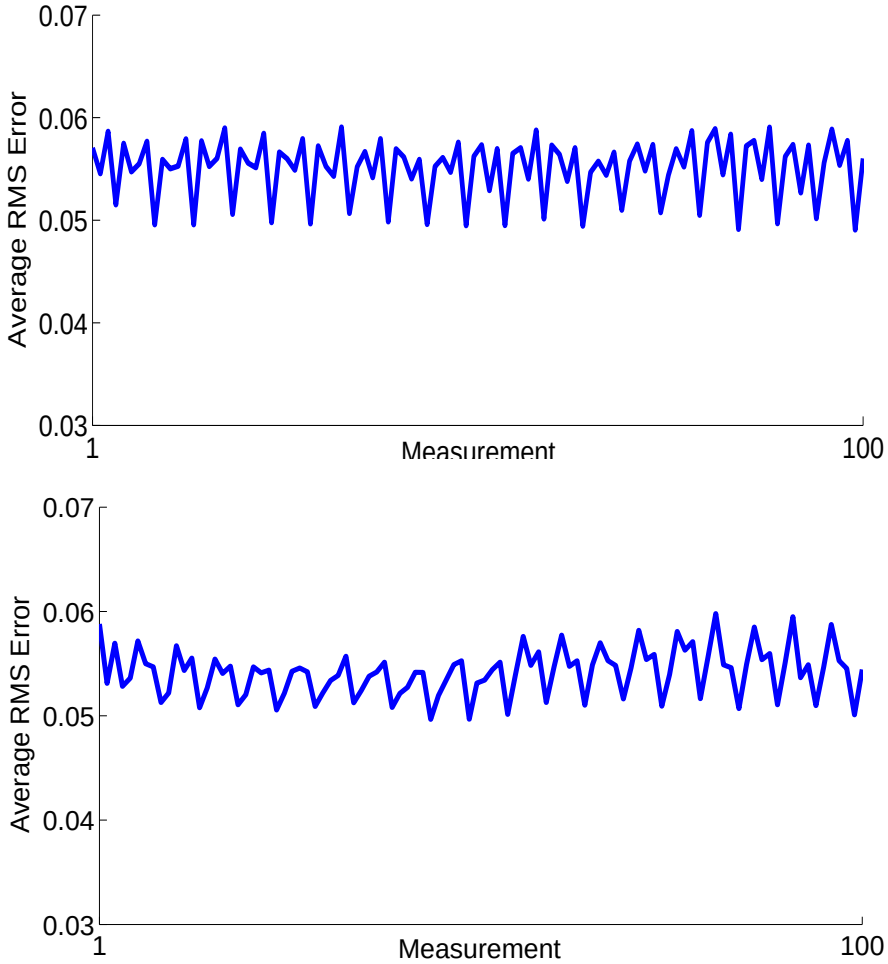

Figure 2.16: Temporal accuracy evaluation. For 100 measurements, distribution of average RMS error of all 24 clips is shown here. Because color wheel rotates 6 rounds for every 5 measurements in our imaging system, a neat pattern of the average RMS error can be obviously observed. Upper: Temporal accuracy using white board; Lower: Temporal accuracy without using white board

lot from the minimum one, by which the stability of proposed method can be guaranteed. Comparing these 2 histograms, it is clear that the difference between them is small. To learn how small the difference is, we can refer 3 kinds of curves shown in Fig. 2.14: black ones indicate the ground truth, red ones indicate the recovered results using white board for illumination recovery and the blue ones indicate the recovered results without using white board for illumination recovery. In all 24 sub-images which correspond the 24 clips, the two recovered results are almost the same, and similar to the ground truth. The 19th clip, the most bright one among all 24 clips, has the biggest mean RMS error which is less than 0.11 and 0.13 respectively. From all the results and corresponding analysis given above, we can draw a conclusion that our system can recover the spectral reflectance at a reasonable accuracy.

Next, we are going to evaluate the temporal accuracy of our system. We reused the 100 measurements used in previous test. For every measurement, we reconstructed the spectral reflectance of all 24 clips; then, the RMS error of the 24 reconstructed results was calculated; after that, we computed the average value of the 24 RMS error values, and used it as the criterion to evaluate each measurement. Just like the spectral accuracy evaluation, one measurement correspond two values because of the different methods for illumination recovery. The distribution of these 2 RMS error values of the 100 measurements are shown in Fig. 2.16. In both results, the average RMS error fluctuates in the same narrow band (0.048, 0.06) by which the temporal accuracy of our system can be verified. Compare with the distribution of average RMS error when we recover illumination without using the white board, the distribution of average RMS error using the white board appears neater. The reason is that when we use the white board, recovered illumination only relies on the appearance of the white board in corresponding image.

Using the other method for illumination recovery, images rely on their mean RGB values. Because the mean RGB values of the Colorchecker is much smaller than the RGB values of the white board, the low SNR (Signal-to-Noise Ratio) causes the distribution a little irregular when without using the white board.

Through above evaluation, it is clear that both the spectral accuracy and the temporal accuracy of our system are not sensitive to the illumination variation cause by different methods for illumination recovery. Though the stability and accuracy of our system can be guaranteed, we still need to know the causes of errors. They may be (1) Although 8 spectral bases can well approximate spectral reflectance of most natural objects, there are still errors between fitting results and ground truth; (2) Because the spectral sensitivity of the high-speed camera is not available from the manufacturer, the function used here is measured by ourselves. The camera works at 500Hz, the shutter speed is only 2ms. Moreover, narrow-band light emitted from monochromator is weak, so the spectral sensitivity shown in Fig. 2.5 may differ from the truth to some extent; (3) Also because of the short exposure time, we need to adjust the digital gain and the analog gain of the camera to make sure the captured images of the scene appear neither too bright nor too dark, the noise caused by these gains would also degrade the recovered results; (4) Because illumination of captured images change from frame to frame, estimated illumination may deviate from the truth, error of estimated illumination would result in error of recovered spectral reflectance; (5) DLP projector used in our system emits RGB 3 distinct light, and the high speed camera output RGB 3 values. Even though the deviation between the spectral distributions of emitted light and spectral sensitivity of the high speed camera enables the 9 measurements for each scene points, these measurements do not equally

contribute to the recovered results. Measurements with big values dominate the final results. Noise of these measurements would cause errors.

2.5 Image and Video Relighting

Spectral relighting is a method to estimate scene's appearance by using recovered surface spectral reflectance, measured spectral sensitivity of sensor and known illumination spectra. Relit results for every scene point is computed by Eq. (2.1). Many works, like Ref. [PLGN07, WHD03], have shown that spectral information of scene is more robust again illumination variation. Through comparing spectral relit results and real captured images, accuracy of recovered spectral reflectance and robustness of our system can be demonstrated. In this section we use the spectral reflectance recovered by our method to do spectral relighting of a static scene as well as moving objects.

2.5.1 Image spectral relighting

In this section, we would show the spectral relit results of a static scene, and compare them with the real captured images. The static scene contains fruits, vegetables, and small statues. Five consecutive frames of the scene were captured by our imaging system. Using them as one measurement, the spectral reflectance of scene points was recovered pixel by pixel. Then, the scene was spectrally relit with a LCD projector (EPSON^{TM} ELP-735) as the light source. The LCD projector was used here to ensure strong and spatial uniformly distributed light. The spectral distributions of its white, red, green, and blue were measured by a spectrometer. Comparison between the relit results and the real captured images is shown in Fig. 2.17. We can

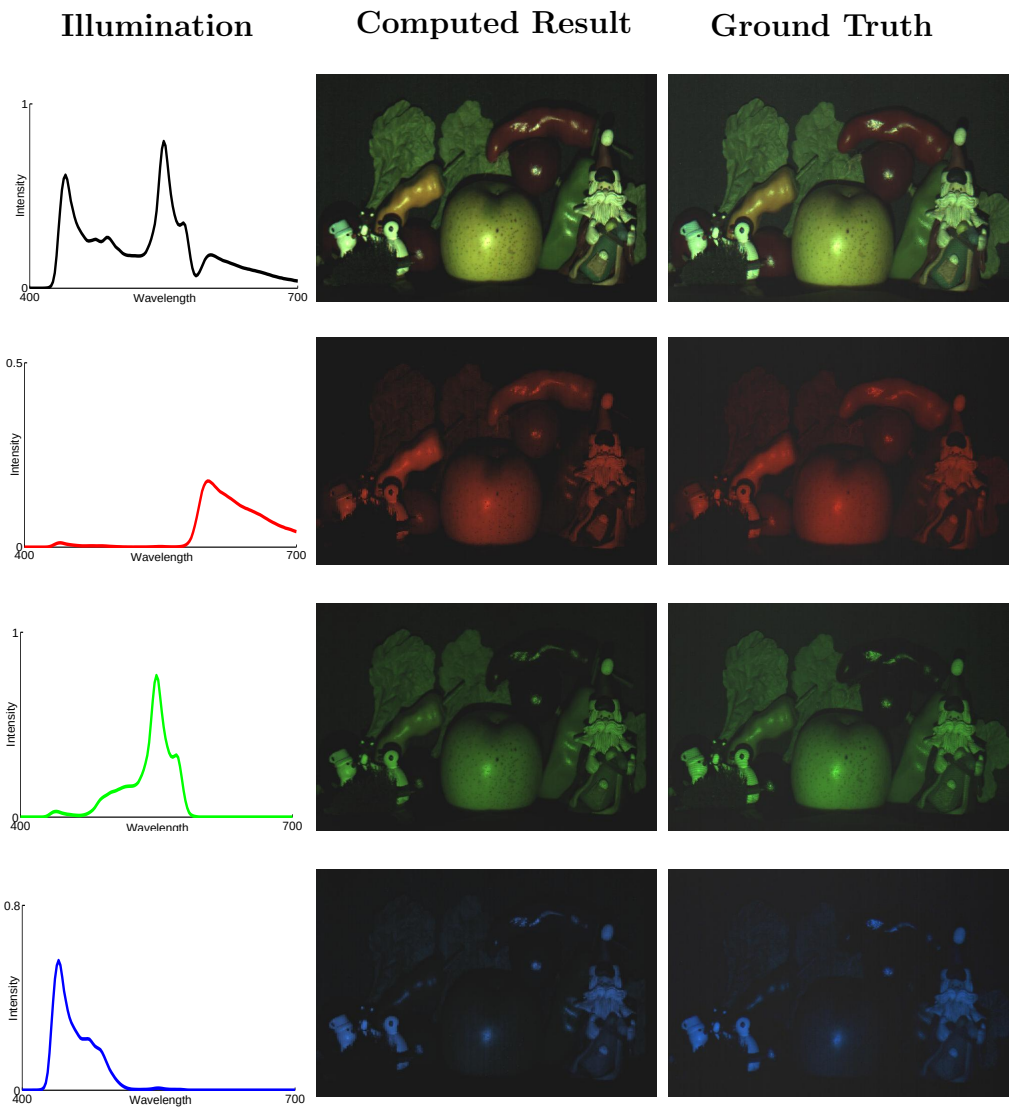

Figure 2.17: Comparison between relit results and captured images of static scene under illuminations from a LCD projector.

see that the computed results are very similar to the ground truth which also reveals the accuracy of our system.

2.5.2 Real video spectral relighting

Our system works at 100 Hz, so it is capable of measuring dynamic scenes. This capability was tested by taking spectral measurements of a rotating globe and a manipulated puppet.

The globe rotates at 10 revolutions per minute. We use our system to take spectral measurement of it. Images contained in one measurement are shown in Fig. 2.18 (a). Next, spectral reflectance of every scene point is recovered by proposed method. Because two methods for illumination recovery are proposed, for the same scene point, two recovered spectral reflectance curves are shown in Fig. 2.18 (b) which are very similar to each other. Then, we do spectral relighting by Eq. (2.1), to compute globe's appearance under a variety of illuminations. Compare Fig. 2.18 (c) and (d), we can see that it is hard to tell the difference between the corresponding images in two sets.

For the puppet, its spectral relighting results are shown in the top two rows of Fig. 2.19. From these results, smooth movement of the puppet can be observed, and its appearance in these images looks natural. Bottom row of Fig. 2.19 simulates what can be captured by a camera works at 30 fps to the same scene. Because the high-speed camera of our system works at 500fps, during the time a 30 fps camera takes a frame, the high-speed camera can capture 16.66 frames. So we synthesize one image that captured by a 30 fps camera through averaging 17 consecutively captured images by the 500 fps camera. Compare the second row and the third row of Fig. 2.19, we can see that motion blur is obvious in the synthesized images, such as the hand in the bottom left image, tie in the bottom middle image, and

(a) One measurement of the rotating globe.

(b) Recovered spectral reflectance of the points on the globe based on the measurement.

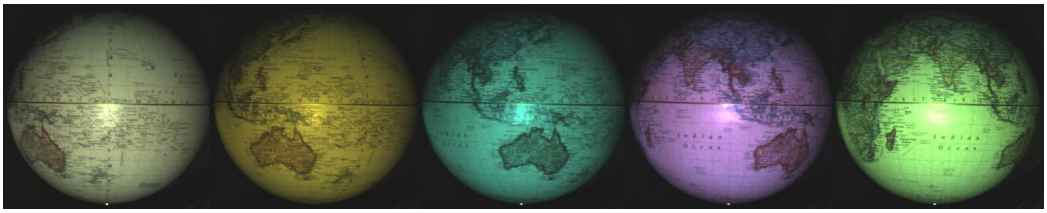

(c) Relit results by the recovered spectral reflectance when using the white board to recover illumination.

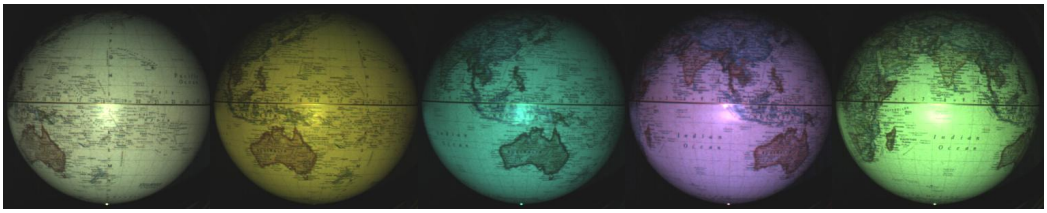

(d) Relit results by the recovered spectral reflectance when recover illumination without using the white board.

Figure 2.18: Recovered spectral reflectance of a rotating globe and relit results.

the eyes in the bottom right image. The corresponding relit results, on the contrary, are degraded little by motion blur. From these comparisons, we can see that our system is more robust to artifacts caused by motion due to its high rate. Therefore, our system can be used for spectral reflectance recovery of dynamic scenes with fast moving objects .

2.6 Conclusion

In this chapter, we exploited the unique color-forming mechanism of DLP projectors. An imaging system for fast spectral reflectance recovery was built by making use of this mechanism. This system is capable of taking measurements as fast as 100 Hz. Every measurement consists of a set of sequentially captured images. For each set, the spectral reflectance of scene points can be recovered.

Through intensive evaluation, the accuracy of our system has been verified. We showed that the spectral accuracy as well as the temporal accuracy are good, and accuracy variation caused by different methods for illumination recovery is small. By image and video spectral relighting, robustness of our system has been confirmed. Moreover, this system is built on easily available devices, and the excellent optical design of DLP projectors guarantees simple calibrations and a large working volume. It can be concluded that our system is practical and robust for the spectral reflectance recovery of fast-moving objects.

Considering more and more DLP projectors are equipped with color wheel of 4, even 6 segments, the proposed method can be used with these DLP projectors without any modification. Theoretically speaking, the use of such projectors should contribute to better over-all accuracy, but requires addi-

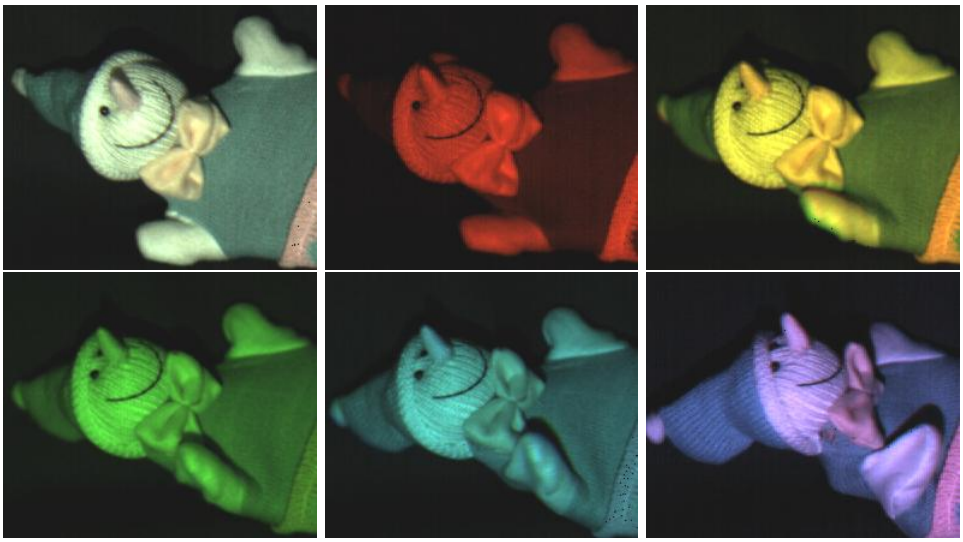

(a) Relit result(100 Hz)

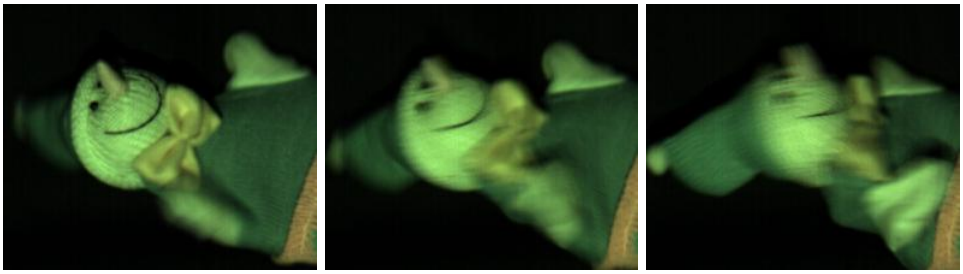

(b) Synthesized image(30 Hz)

Figure 2.19: (a): relit results of fast-moving puppet. The continuous movements through very different illuminations can be computed using by the recovered spectral reflectance. (b): synthesized result to simulate captured image by a 30 fps camera in which motion blur degrades image quality severely.

tional effort to calibrate the system, *i.e.*, measuring the spectral property of each color segment.

Chapter 3

Camera spectral sensitivity estimation without illumination spectrum

3.1 Background

Light spans a wide range of wavelengths. With a digital color camera, the scene radiance is recorded as RGB values via color filters that specify light in different wavelength ranges to be observed. Therefore, the recorded RGB values are dependent on the spectral sensitivity of color filters (or sensors); *i.e.*, different sensors yield different RGB outputs for the same scene. Camera spectral sensitivity is an indispensable factor for a lot of computer vision tasks that use color information, such as spectral reflectance recovery [CHM10, PLGN07], color correction [MPW06] and color constancy [FHH01, For90]. That means estimation of camera spectral sensitivity is necessary to guarantee various color-based methods work well.

A standard technique for estimating camera spectral sensitivity is to take

pictures of monochromatic light whose bandwidth is narrow [Ass10]. The spectral sensitivity of the camera can be reliably estimated from recorded observations and known spectral distributions of monochromatic light. Although it gives accurate estimates, the method requires expensive hardware to generate and measure monochromatic light, thus its use has been limited to well-equipped laboratories only. In addition, the calibration procedure is laborious because of the need for multiple observations of different light.

To simplify the procedure, methods using calibration targets whose reflectance are known have been proposed [FHH98, UDHS10, MAR11]. These methods estimate the camera spectral sensitivity by recording a calibration target, *e.g.*, IT8 Target, under illumination with a known spectral distribution. These approaches reduce the effort needed for calibration. However, their requirement for a known illumination spectrum limits their practicability due to the need for a spectrometer or a strong assumption to be placed on the illumination spectrum.

In this paper, we propose a new method for estimating the camera spectral sensitivity from a single image captured under an *unknown* illumination. The key idea is to use fluorescence: a physical phenomenon whereby the substance emits specific wavelengths of light by absorbing radiation of different wavelengths. Its physical property of a fixed emission spectrum is particularly useful for the camera spectral sensitivity estimations because the spectral profile of the fluorescence remains unchanged up to a certain scale under arbitrary illumination. To make a single image estimate, we use a chart of fluorescent materials whose emission spectra are pre-determined. Then, from the emission spectra of these fluorescent materials, we derive an analytic solution for determining the camera spectral sensitivity.

There are three key properties about the proposed method. First, it

does not require the illumination spectrum to be known. The estimate can be made under unknown lighting conditions, *e.g.*, outdoors under sunlight, under a skylight, or indoors under a fluorescent lamp, without having to measure any spectra. Second, the estimation requires only a single shot of a scene with the calibration target. This reduces the cost of data acquisition. Third, the fluorescent chart used here is made from fluorescent paint, which is inexpensive and readily available at stationery stores. These properties will make the camera spectral sensitivity estimation more widely available.

The rest of this chapter is organized as follows. Section 3.2 gives a brief review of related works. Section 3.3 presents chromaticity invariance of fluorescence. Section 3.4 shows a method to separate fluorescent component from reflective component in captured images. In section 3.5, camera spectral sensitivity is represented by Fourier bases; a method to estimate corresponding coefficients is introduced. Estimated results under different illuminations and applications of estimated camera spectral sensitivity are shown in Section 3.6. Finally, we conclude this chapter in Section 3.7.

3.2 Related works

Camera spectral sensitivity can be estimated by establishing a relationship between incident narrow-band light with different wavelengths across the visible wavelength range and the camera's outputs. To achieve this goal, the standard technique uses a monochromator or narrow-band filters to generate a series of monochromatic light. Each monochromatic light is cast on a standard white board, and the reflected light is observed by the target camera. At the same time, the spectral distributions of the monochromatic light are measured by a spectrometer. The camera spectral sensitivity can

then be calculated using the captured images and measured spectra [Ass10]. Because measurements are independent of each other, this method is accurate. However, it requires expensive optical equipments and a dark room. Moreover, capturing dozens of images and spectral distributions makes the whole procedure time-consuming.

To make measurement more practical, methods using calibration targets are proposed. These calibration targets, *e.g.*, the IT8 target or Macbeth ColorChecker, contain several patches whose spectral reflectance is known. Under illumination with known spectrum, spectra of reflected light from these patches can be computed. The camera spectral sensitivity can also be computed from the RGB values of these patches in captured images [FHH98, BF02, Ebn07, UDHS10]. However, these methods require controlled lighting conditions, which means the light should be spatially uniform and its spectral distribution is known. These requirements can be satisfied only in laboratories. To extend the scope of these methods out of the lab, Rump *et al.*devised an imaging model accounting for specularity and spatially varying illumination [MAR11]. By using this model, measurements can be conducted in an environment where specularity or shadows exist. However, it still needs a known illumination spectrum.

To avoid the requirement for a known illumination spectrum, we make use of fluorescence. Fluorescence has been receiving more and more attention recently. In [JF99, HHA+10], methods describing how to model and render fluorescent materials are presented. Modified color constancy methods to deal with fluorescent surfaces are shown in [Bar99]. In [HFI+08], fluorescence is used to sample the geometry of transparent objects that cannot be sampled with traditional methods. In this chapter, we explore the spectral properties of fluorescence; and use them to estimate the camera spectral sensitivity.

3.3 Fluorescence

Fluorescence is a common phenomenon which has been used for a variety of purposes, such as in lamps, stationery, safety vests, *etc.* Fluorescence is the emission of light by a substance that has absorbed light of different (generally shorter) wavelengths. In this absorption and re-emission process, two terms about fluorescence are involved: absorption (or excitation) spectrum and emission spectrum. The absorption spectrum represents how strongly the fluorescent material absorbs fluorescence-exciting light as a function of its wavelength. The emission spectrum describes the spectral profile of fluorescence emitted from the fluorescent material. Both of the absorption spectrum and emission spectrum are determined by the properties of the fluorescent material itself.

The emitted fluorescence from the p-th fluorescent material, $f_p(\lambda)$ ($p = 1, 2, 3, ..., P$), is described as

$$f_p(\lambda) = \left(\int a_p(\lambda') l(\lambda') d\lambda' \right) e_p(\lambda), \tag{3.1}$$

where λ' and λ are the wavelengths of the incoming light and the outgoing fluorescence, $a_p(\lambda')$ and $e_p(\lambda)$ are the absorption and emission spectra of the p-th fluorescent material, $l(\lambda')$ is the spectral distribution of the incoming light.

We can see that the integral part in Eq. (3.1) is determined by the absorption spectrum and the spectrum of the incoming light. Therefore, it is independent from the spectrum of the outgoing fluorescence. Replacing that part by a scale factor k_p, we can rewrite Eq. (3.1) as

$$f_p(\lambda) = k_p e_p(\lambda). \tag{3.2}$$

Eq. (3.2) means that the emitted fluorescence from a certain fluorescent material under different illuminations remains unchanged up to a certain scale.

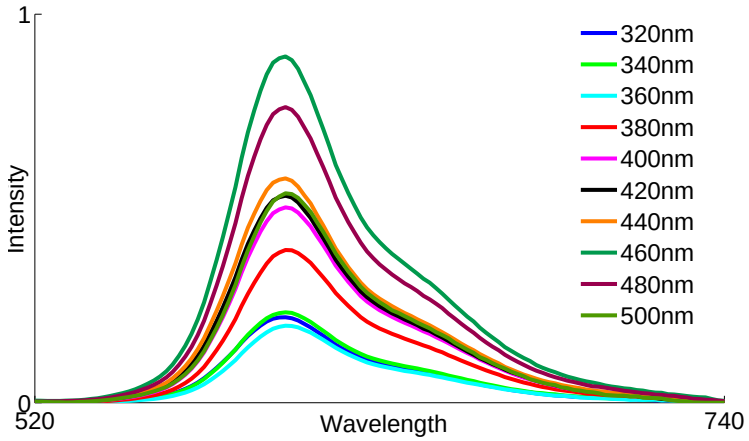

Figure 3.1: Spectral distributions of emitted fluorescence from the same material under different monochromatic light remain unchanged up to a certain scale.

To verify this unique property of fluorescence, we measured the fluorescence emitted from a patch smeared with fluorescent paint under different monochromatic light. The measured spectral distributions are shown in Fig. 3.1. As expected from Eq. (3.2), all these distributions are different only in scales.

When the emitted fluorescence from the p-th fluorescent material is observed with an RGB camera, the relationship between the pixel intensity $(R_p^f, G_p^f, B_p^f)^T$ and the emitted fluorescence is represented by

$$R_p^f = \int f_p(\lambda) c_R(\lambda) d\lambda. \tag{3.3}$$

Here, $c_R(\lambda)$ ($c_G(\lambda)$ and $c_B(\lambda)$) is the spectral sensitivity of the red channel (green channel and blue channel). G_p^f and B_p^f can be represented in a similar manner. we assume the camera has linear intensity response function. Without loss of generality, geometric factors can be omitted. For the sake of simplicity, we hereafter derive equations for red channel and omit those for green and blue channels if they are trivial.

Substituting Eq. (3.2) into Eq. (3.3), we obtain

$$R_p^f = k_p \int e_p(\lambda) c_R(\lambda) d\lambda. \tag{3.4}$$

Note that the scale factor k_p is the same for all three channels. Then, the chromaticity $(r_p^f, g_p^f, b_p^f)^T$ of the emitted fluorescence is described as

$$\begin{aligned} r_p^f &= \frac{R_p^f}{R_p^f + G_p^f + B_p^f} \\ &= \frac{\int e_p(\lambda) c_R(\lambda) d\lambda}{\int e_p(\lambda)(c_R(\lambda) + c_G(\lambda) + c_B(\lambda)) d\lambda}. \end{aligned} \tag{3.5}$$

The other components g_p^f and b_p^f can be described in a similar manner. We can see that the scale factor k_p is eliminated. As a result, the chromaticity of the emitted fluorescence is invariant with respect to the spectrum of the incoming light.

Using the chromaticity invariance of emitted fluorescence is the key idea of our method. It enables us to estimate the spectral sensitivity of a camera without having to know the illumination spectrum.

3.4 Separating fluorescent and reflective components

As discussed in Section 3.3, the chromaticity of emitted fluorescence is invariant with respect to changes in illumination. Unfortunately, however, fluorescent materials often not only emit fluorescence but also reflect light. Thus, the observed pixel intensity of the p-th fluorescent material, $(R_p, G_p, B_p)^T$, contains a fluorescent component $(R_p^f, G_p^f, B_p^f)^T$ as well as a reflective component $(R_p^r, G_p^r, B_p^r)^T$:

$$R_p = R_p^f + R_p^r. \tag{3.6}$$

Therefore, we need to separate these components in order to make use of the chromaticity invariance of the fluorescent component. Recently, Zhang and Sato [ZS11] proposed a method for separating fluorescent and reflective components by using independent component analysis, but their method requires at least two images captured under different illuminations.

In this section, we show how to separate the fluorescent and reflective components from a single image. The key idea is to use non-fluorescent materials with known spectral reflectance as a reference (Fig. 3.2).

We first estimate the reflective components of fluorescent materials from those of the non-fluorescent materials under an unknown illumination. The reflective component is described as

$$R_p^r = \int s_p(\lambda) c_R(\lambda) l(\lambda) d\lambda, \tag{3.7}$$

where $s_p(\lambda)$ is the spectral reflectance of the p-th fluorescent material. G_p^r and B_p^r can be described in a similar manner. According to a previous study [PHJ89], the spectral reflectance of various materials can be approximately represented by a linear combination of a small number of basis functions. Thus, we have

$$s_p(\lambda) = \sum_{n=1}^{N} \alpha_{p,n} b_n^r(\lambda), \tag{3.8}$$

where $b_n^r(\lambda)$ $(n = 1, 2, 3, ..., N)$ are the basis functions for spectral reflectance that available in [PHJ89], and $\alpha_{p,n}$ are the corresponding coefficients. Substituting Eq. (3.8) into Eq. (3.7), we obtain

$$R_p^r = \sum_{n=1}^{N} \alpha_{p,n} \int b_n^r(\lambda) c_R(\lambda) l(\lambda) d\lambda. \tag{3.9}$$

If we know $\alpha_{p,n}$ and $\int b_n^r(\lambda) c_R(\lambda) l(\lambda) d\lambda$, the reflective components R_p^r can be computed. Because our objective is to design a calibration target, the reflectance $s_p(\lambda)$ can be measured in advance. So, the coefficient can

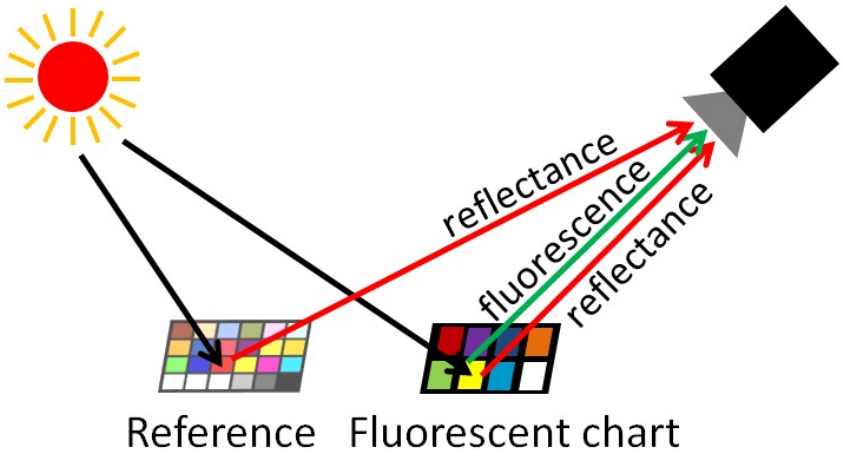

Figure 3.2: Under spatial uniformly distributed illumination, a reference containing a number of non-fluorescent patches with known spectral reflectance is used to help separating the fluorescent component from the reflective component of the captured images of the fluorescent chart.

be computed as $\alpha_{p,n} = \int s_p(\lambda) b_n^r(\lambda) d\lambda$ since the basis functions are known and orthogonal to each other. Hence, the remaining problem is how to get $\int b_n^r(\lambda) c_R(\lambda) l(\lambda) d\lambda$. To solve this problem, a reference containing a number of non-fluorescent materials with known spectral reflectance is used.

A color image of the reference is captured together with fluorescent chart under the same illumination as shown in Fig. 3.2. Then, the observed pixel intensity of the q-th reference material, $(R_q, G_q, B_q)^T$ $(q = 1, 2, 3, ..., Q)$, is represented by

$$R_q = \sum_{n=1}^{N} \alpha_{q,n} \int b_n^r(\lambda) c_R(\lambda) l(\lambda) d\lambda. \tag{3.10}$$

Here, $\alpha_{q,n}$ are known and $\int b_n^r(\lambda) c_R(\lambda) l(\lambda) d\lambda$ are unknown. For all materials on the reference, we obtain a set of linear equations that are similar to Eq. (3.10). The number of equations is Q (reference materials) $\times$ 3 (channels), and the number of unknowns is N (basis functions) $\times$ 3 (channels).

When $Q \geq N$, the unknown integral $\int b_n^r(\lambda)c_R(\lambda)l(\lambda)d\lambda$ can be estimated. Because we set $N = 8$ according to the previous study [PHJ89], the reference chart should contain at least eight materials whose spectral reflectance is linearly independent.

Once we obtain the integral in Eq. (3.10), the reflective components of the fluorescent materials can be calculated by Eq. (3.9). Finally, the fluorescent components $(R_p^f, G_p^f, B_p^f)^T$ are computed by subtracting the calculated reflective components from the observed pixel intensities as

$$R_p^f = R_p - R_p^r. \tag{3.11}$$

3.5 Estimating camera spectral sensitivity

In the previous sections, we described that the chromaticity of fluorescence is invariant under different illuminations and that the fluorescent components can be extracted by using non-fluorescent materials as a reference even under an unknown illumination. In this section, we show how to use the illumination-invariant chromaticity of the fluorescent components for estimating the camera spectral sensitivity.

Though different cameras have different spectral sensitivities, their spectral sensitivities should not deviate a lot from each other. Thus, it becomes possible to use a limited number of parameters or basis functions to express camera spectral sensitivity. To estimate spectral sensitivity, we just need to estimate the parameters or corresponding coefficients [FHH98, TW01]. To guarantee the general applicability of our method, we adopt Fourier basis functions. Assuming the range of spectral sensitivity is $[\lambda^l, \lambda^u]$, the first few Fourier basis functions are $b_1^c(\lambda) = 1$, $b_2^c(\lambda) = \sin[2\pi(\lambda - \lambda^l)/(\lambda^u - \lambda^l)]$, $b_3^c(\lambda) = \cos[2\pi(\lambda - \lambda^l)/(\lambda^u - \lambda^l)]$ *etc.* We could also use eigenvectors com-

puted from a set of camera spectral sensitivities if such data are available. Accordingly, the spectral sensitivity $(c_R, c_G, c_B)^T$ can be decomposed into a sum of sines and cosines as

$$c_R(\lambda) = \sum_{m=1}^{M} \beta_{R,m} b_m^c(\lambda), \tag{3.12}$$

where $b_m^c(\lambda)$ are the Fourier bases for representing the camera spectral sensitivity. $\beta_{R,m}$ are the corresponding coefficients for the red channel. The spectral sensitivities of the green and blue channels, c_G and c_B, can be decomposed in a similar manner.

Different numbers of bases have different fitting accuracies. To evaluate how well different number of Fourier bases are capable of fitting spectral sensitivities of different cameras, we use a camera spectral sensitivity database which contains spectral sensitivities of 12 different cameras [Sen]. For each camera, we use 5, 7, 9, 11 Fourier bases to fit its spectral sensitivity of RGB 3 channels respectively; then, computer the average value of RMS error of RGB 3 channels. Results are shown in Tab. 2.

We can see that the more bases we use, the higher accuracy we can get, reconstructed results of Canon 5D by using different number of Fourier bases are shown in Fig. 3.3.

Substituting Eq. (3.12) into Eq. (3.5), we obtain

$$r_p^f = \frac{\sum_m \beta_{R,m} \int e_p(\lambda) b_m^c(\lambda) d\lambda}{\sum_m (\beta_{R,m} + \beta_{G,m} + \beta_{B,m}) \int e_p(\lambda) b_m^c(\lambda) d\lambda}. \tag{3.13}$$

Denoting the integral $\int e_p(\lambda) b_m^c(\lambda) d\lambda$ by $t_{p,m}$, we can rewrite Eq. (3.13) as

$$\begin{bmatrix} (r_p^f - 1)\boldsymbol{t}_p & r_p^f \boldsymbol{t}_p & r_p^f \boldsymbol{t}_p \end{bmatrix} \begin{bmatrix} \boldsymbol{\beta}_R \\ \boldsymbol{\beta}_G \\ \boldsymbol{\beta}_B \end{bmatrix} = 0, \tag{3.14}$$

where $\boldsymbol{t}_p = (t_{p,1}, \cdots, t_{p,M})$ is a $1 \times M$ row vector; $\boldsymbol{\beta}_R = (\beta_{R,1}, \cdots, \beta_{R,M})^T$ is a $M \times 1$ column vector, $\boldsymbol{\beta}_G$ and $\boldsymbol{\beta}_B$ are defined in a similar manner. Similar

Camera Model	5-basis	7-basis	9-basis	11-basis
KODAK DCS 420	0.0715	0.0431	0.0325	0.0281
SONY DXC 930	0.0523	0.0252	0.0169	0.0118
NIKON D1X	0.0796	0.0376	0.0227	0.0173
SONY DXC 9000	0.0705	0.0313	0.0180	0.0085
CANON 10D	0.0627	0.0261	0.0164	0.0099
NIKON D70	0.0627	0.0320	0.0167	0.0088
KODAK DCS 460	0.0706	0.0538	0.0479	0.0444
CANON 400D	0.0875	0.0632	0.0583	0.0517
CANON 5D	0.0656	0.0322	0.0224	0.0165
CANON 5D Mark 2	0.0664	0.0335	0.0271	0.0211
Ladybug2	0.1099	0.0631	0.0542	0.0406
KODAK DCS 200	0.0751	0.0533	0.0349	0.0195

Table 3.1: Average RMS error of reconstructing camera spectral sensitivity by using different numbers of Fourier bases.

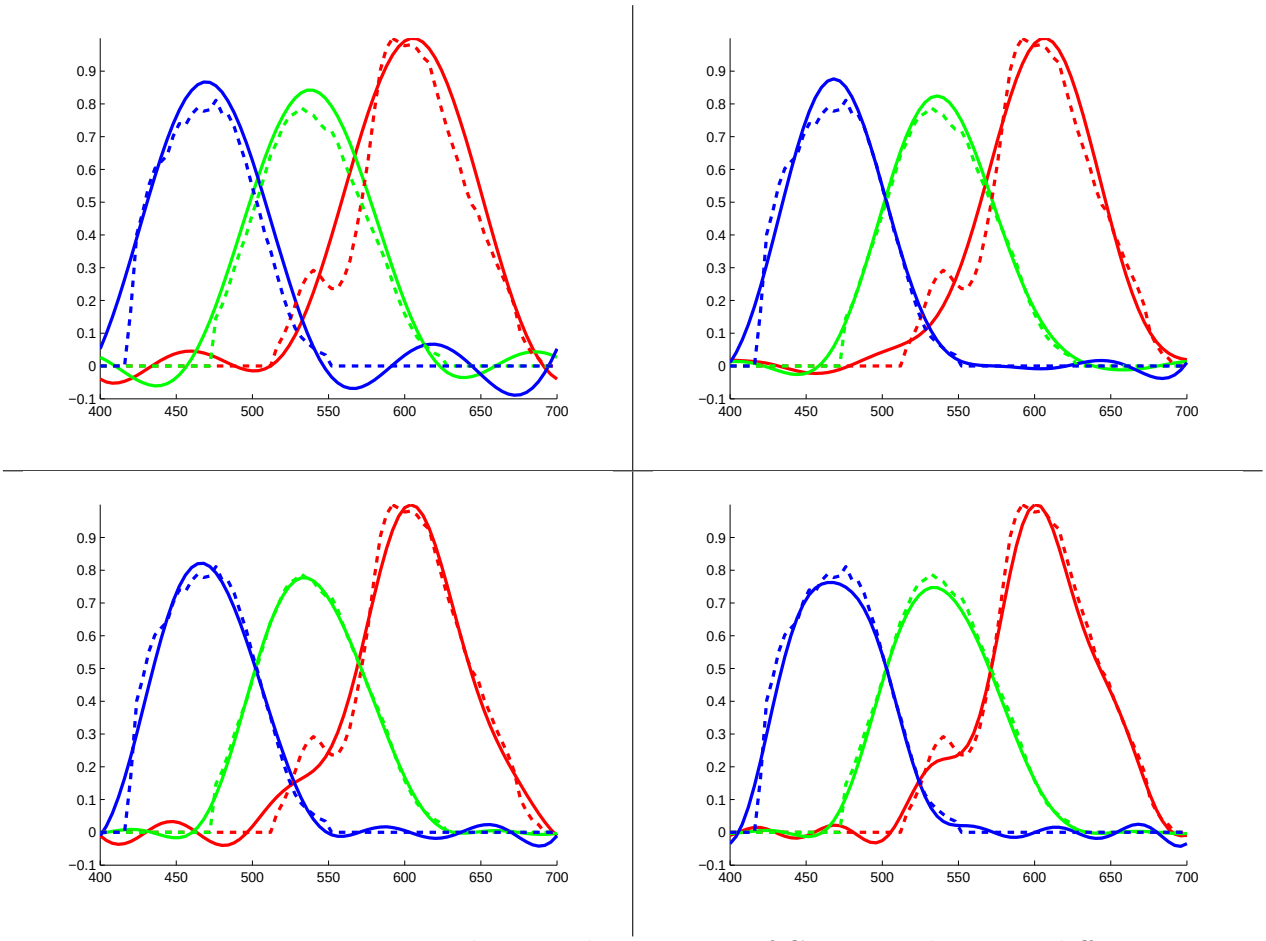

Figure 3.3: Reconstructed spectral sensitivity of Canon 5D by using different number of Fourier bases. Dotted curves: ground truth; Solid curves: fitting results. Left upper: using 5-basis; Right upper: using 7-basis; Left lower: using 9-basis; Right lower: using 11-basis.

equations can be obtained for the green and blue channels. Since there are P fluorescent materials, we have P (fluorescent materials) $\times$ 3 (channels) equations in total:

$$\begin{bmatrix} (r_1^f - 1)\boldsymbol{t}_1 & r_1^f \boldsymbol{t}_1 & r_1^f \boldsymbol{t}_1 \\ g_1^f \boldsymbol{t}_1 & (g_1^f - 1)\boldsymbol{t}_1 & g_1^f \boldsymbol{t}_1 \\ b_1^f \boldsymbol{t}_1 & b_1^f \boldsymbol{t}_1 & (b_1^f - 1)\boldsymbol{t}_1 \\ \vdots & \vdots & \vdots \\ (r_P^f - 1)\boldsymbol{t}_P & r_P^f \boldsymbol{t}_P & r_P^f \boldsymbol{t}_P \\ g_P^f \boldsymbol{t}_P & (g_P^f - 1)\boldsymbol{t}_P & g_P^f \boldsymbol{t}_P \\ b_P^f \boldsymbol{t}_P & b_P^f \boldsymbol{t}_P & (b_P^f - 1)\boldsymbol{t}_P \end{bmatrix} \begin{bmatrix} \boldsymbol{\beta}_R \\ \boldsymbol{\beta}_G \\ \boldsymbol{\beta}_B \end{bmatrix} = 0. \tag{3.15}$$

Eq. (3.15) can be expressed in the form of $\boldsymbol{AX} = 0$, where $\boldsymbol{A}$ is a $3P \times 3M$ matrix and $\boldsymbol{X}$ is a $3M \times 1$ vector. A nonzero solution of this linear equation is found as the eigenvector of the square matrix $\boldsymbol{A}^T\boldsymbol{A}$ corresponding to the smallest eigenvalue.

In experiments, we found that the estimated coefficients $(\boldsymbol{\beta}_R, \boldsymbol{\beta}_G, \boldsymbol{\beta}_B,)^T$ are sometimes sensitive to noise. Therefore, to make the computation more stable, we incorporate a smoothness constraint on spectral sensitivity. The second derivative of spectral sensitivity with respect to wavelength is used as the smoothness constraint, and as a result we obtain

$$\begin{bmatrix} & \boldsymbol{A} & \\ w_R\boldsymbol{\phi} & \boldsymbol{0} & \boldsymbol{0} \\ \boldsymbol{0} & w_G\boldsymbol{\phi} & \boldsymbol{0} \\ \boldsymbol{0} & \boldsymbol{0} & w_B\boldsymbol{\phi} \end{bmatrix} \boldsymbol{X} = 0, \tag{3.16}$$

where $(w_R, w_G, w_B)^T$ is the weight of the smoothness term and $\boldsymbol{\phi} = (d^2 b_1^c(\lambda)/d\lambda^2, \cdot\cdot\cdot, d^2 b_M^c(\lambda)/d\lambda^2)$. Substituting the solution of Eq. (3.16) into Eq. (3.12), camera spectral sensitivity can be obtained up to a scale.

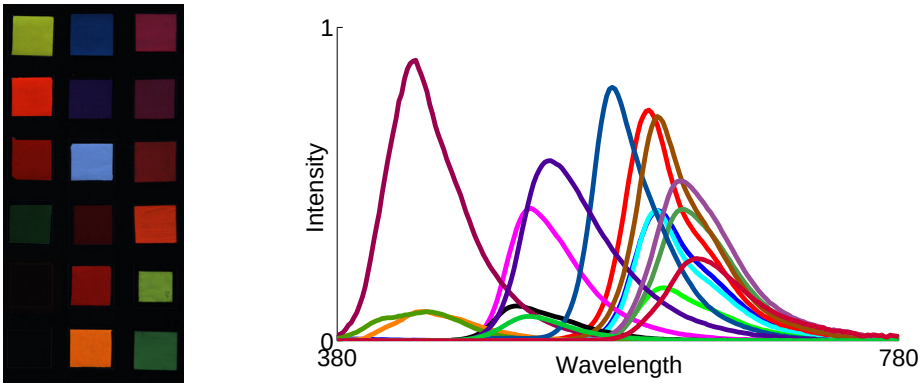

Figure 3.4: Left: used fluorescent chart; Right: spectral distributions of fluorescence emitted from its 16 patches.

The steps for camera spectral sensitivity is summarized as: (1) take a picture of the fluorescent chart and the reference; (2) separate the fluorescent and the reflective components of the fluorescent chart in the captured image; (3) compute the chromaticity of the fluorescent component; (4) estimate the camera spectral sensitivity as described in this section; (5) normalize the estimated camera spectral sensitivity, by which the largest absolute value of the estimated results in RGB channels is set to one.

3.6 Experimental results

In this section, we show experimental results to evaluate our method for estimating camera spectral sensitivity as well as two applications of our method: daylight spectrum estimation and color correction.

A chart containing 16 patches, shown in Fig. 3.4, was used in our experiments. Those patches were made on a black board by smearing 16 different types of fluorescent paint ($P = 16$) easily available from stationary stores. To measure the emission spectrum of each fluorescent patch, it was lit by 320nm

UV light generated by a monochromator (SHIMADZU^{TM} SPG-120), and the spectral distribution of light from the patch was measured by a spectrometer (PhotoResearch^{TM} PR-670). Because no light in the visible wavelength range was emitted from the monochromator, the measured results (Fig. 3.4) are the spectral distributions of fluorescence $f_p(\lambda)$.

As stated in Section 3.4, a non-fluorescent reference is used for separating fluorescent and reflective components. In our experiments, we used a Macbeth ColorChecker with 24 patches whose spectral reflectance is publicly available [Mac]. For the spectral reflectance of fluorescent patches, we use the method proposed in [Don54]. To each fluorescent patch, we build its bispectral radiance factor matrix (Donaldson matrix). Spectral reflectance of the fluorescent patch can be represented by the diagonal elements of the matrix.

We estimated the spectral sensitivities of three different cameras by taking pictures under four common illuminations: sun, blue sky, cloudy sky, and fluorescent-lamp. The spectral distributions of these illuminations were unknown. Based on the previous study [FHH98], 9 Fourier basis functions plot in Fig. 3.5 are used for representing camera spectral sensitivity. To test how well these 9 Fourier bases are capable of approximating cameras' spectral sensitivity, some fitting results are shown in Fig. 3.6. From them, we can learn that 9 Fourier bases can approximate spectral sensitivity of different cameras with good accuracy.

Besides using 9 9 Fourier bases, we set the weight of the smoothness term to $(8, 8, 3)^T$. The Estimated results using our method are shown as continuous curves in Fig. 3.6. The Results by using monochromatic lights are shown as dotted curves. To evaluate the difference between them, for each estimated result, we computed the average value of the root mean square

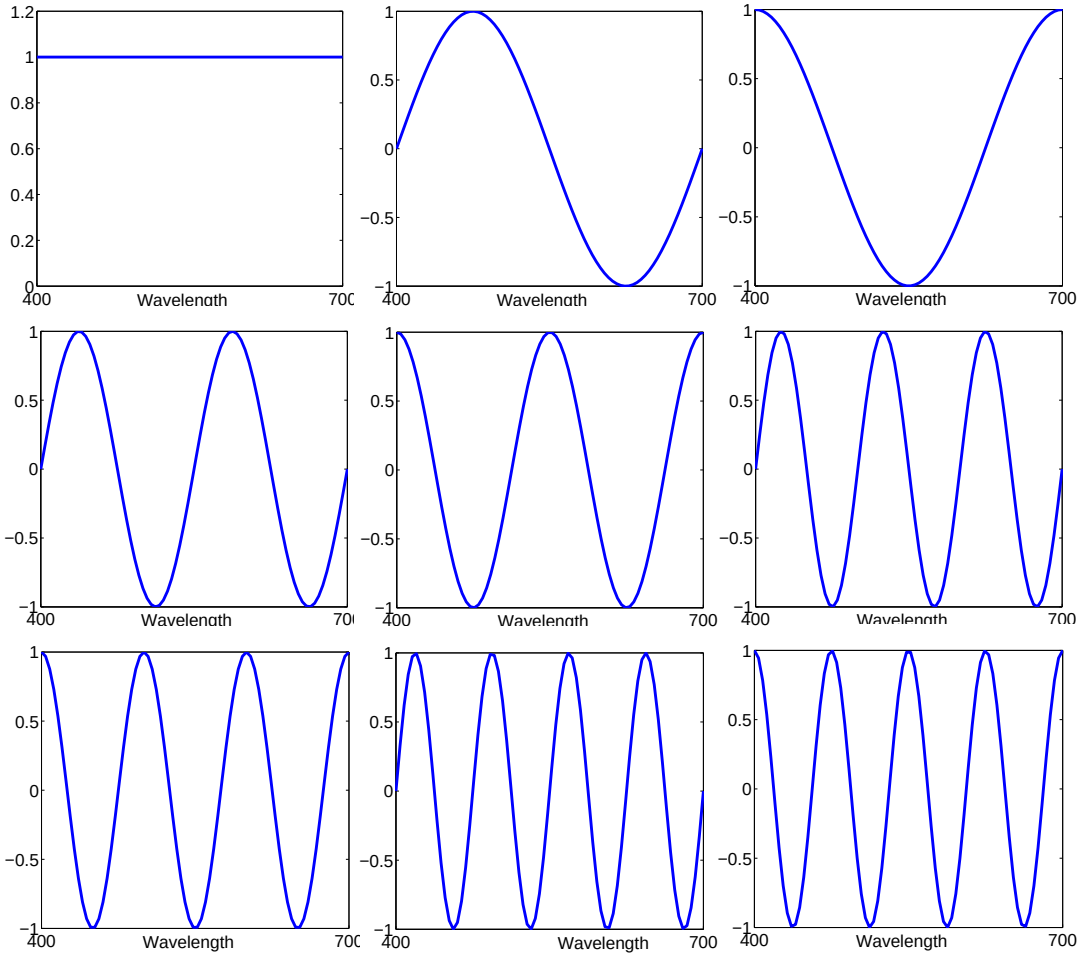

Figure 3.5: 9 Fourier bases used to approximate camera spectral sensitivity

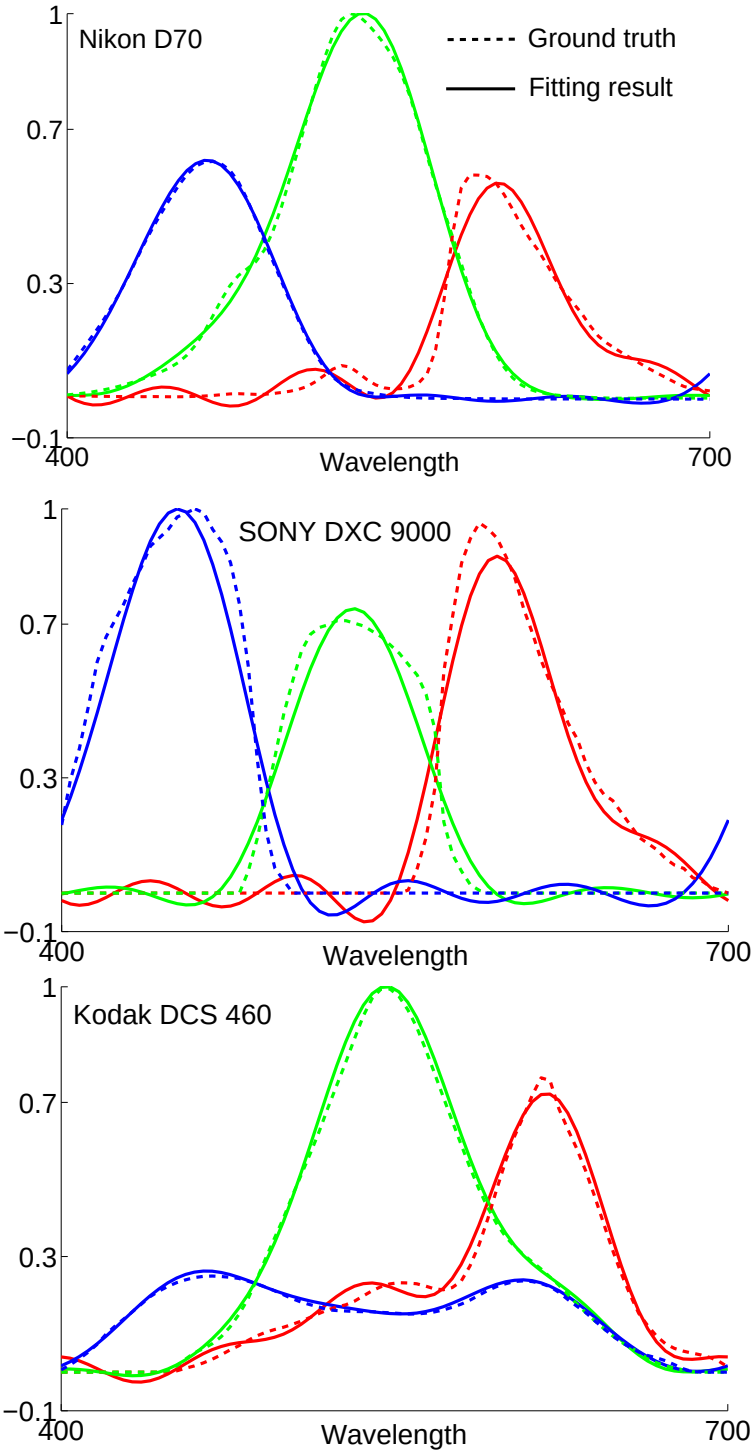

Figure 3.6: Fitting results using 9 Fourier bases

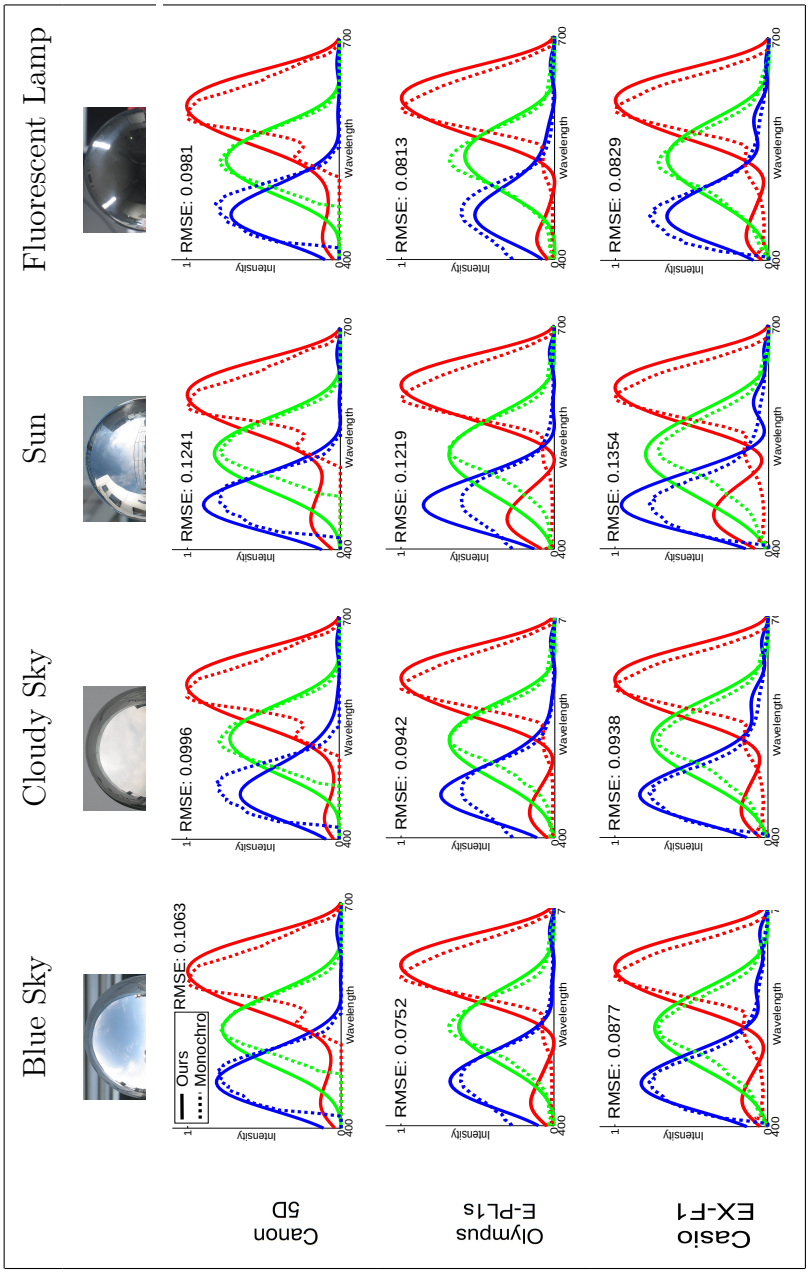

Figure 3.7: Estimated spectral sensitivities of cameras under different illuminations whose spectra are unknown. Results of our method are similar to those using monochromatic light, but ours have less high frequency because of the use of Fourier bases and the smooth constraint.

errors (RMSE) of all 3 channels. The numbers are also shown Fig. 3.6. These results show the accuracy of our method even without knowing the illumination spectra.

Observing the estimated results of our method, we can see that the results under sunlight have a little bigger errors than those under the other illuminations. The reason behind this is the fact that fluorescent materials absorb light with higher energy than their emitted fluorescence. As shown in Fig. 4.3, to light from the blue sky or the cloudy sky, its intensity in the shorter wavelength range (higher energy) is stronger than that in the longer wavelength range (lower energy). On the contrary, sunlight is stronger in the longer wavelength range. Hence, the fluorescent component of the fluorescent chart under the sunlight is darker than those under the other illuminations. This results in that the estimated results under sunlight by our method are more easily affected by noise and errors. Therefore, when using our method, illuminations which are strong in high energy wavelength range, *e.g.*, skylight, are recommended.

Another observation about the estimated camera spectral sensitivities is that: results of the blue channel show larger deviations when compared with those of the green and red channels. Our explanation is that fluorescent materials which emit blue fluorescence require stronger UV light and absorb less visible light, thus their fluorescent components always appears darker than the other patches under common illuminations. Our estimates for the blue channel are thus more easily affected by noise or errors than the other two channels.

3.7 Conclusion

In this chapter, we proposed a single-image method for camera spectral sensitivity estimation. Comparing with existing methods, our method has no

requirement for known illumination spectra. In other words, the estimation can be carried out under unknown illumination.

This benefit results from the using of fluorescence. Under different illuminations, spectral distributions of fluorescence emitted from the same fluorescent material remain unchanged up to a certain scale. Making use of chromaticity invariance of fluorescence, illumination spectra are no longer necessary for estimation of camera spectral sensitivity. We build a calibration chart by several kinds of fluorescent paint whose emission spectrum is calibrated already. Taking a single picture of it as well as a Macbeth ColorChecker under unknown illumination, spectral sensitivity of the camera can be estimated. The effectiveness of the proposed method was successfully demonstrated with experiments using real images taken under various illumination conditions.

In the future, we are planning to work on how to select a set of fluorescent paint to achieve better estimation accuracy under a wide range of illumination conditions.

Chapter 4

Daylight spectrum estimation

4.1 Background

In chapter 3, we discussed how to estimate spectral sensitivity of cameras. Using the estimated camera spectral sensitivity, we talk about estimation of daylight spectra in this chapter. Therefore, this chapter can be seen as an extension of chapter 3

In chapter 3, a Macbeth ColorChecker is used as a reference chart. Appearance of its patches in captured images relies on spectral reflectance of the patches, camera spectral sensitivity as well as illumination. For the spectral reflectance is known, camera spectral reflectance is estimated, illumination estimation becomes possible. Here, we limit the range to daylight spectra rather than general illumination due to the contradiction between the low dimensionality of reflectance and the high dimensionality of illumination. On the one hand, dimensionality of objects has been proved to be 8 [PHJ89]. On the other hand, more and more man-made light sources are used in our ordinary life, such as Organic Light-Emitting Diodes (OLED) and Electro Luminescence (EL). Because of their different light-emitting mechanisms, as

Spectrum of skylight

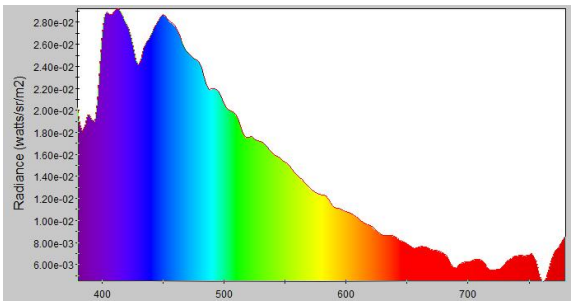

Spectrum of D65

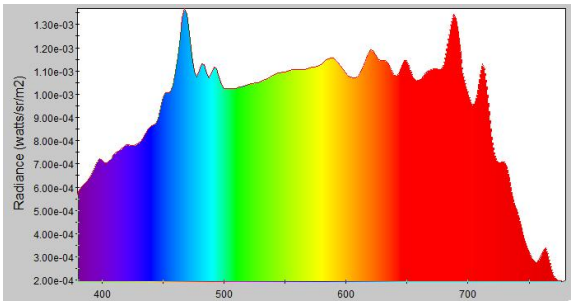

Spectrum of fluorescent lamp

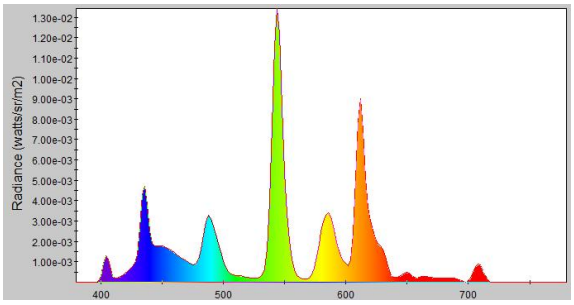

Spectrum of light emitted from LCD projector when input [255,255,255]

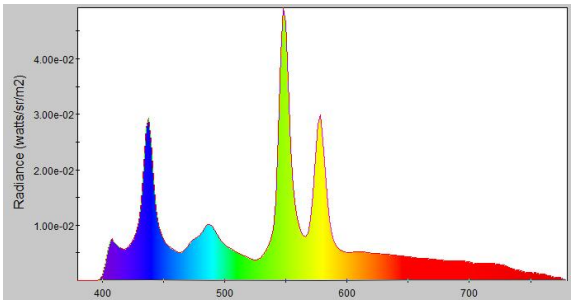

Figure 4.1: Spectral distributions of 4 kinds of illumination in visible wavelength range: $[380, 780]nm$.

shown in Fig. 4.1, spectral distributions of emitted light from them are different from each other. Reflection can not provide enough measurements for illumination estimation in general term. Although some linear models are proposed to approximate illumination including both of natural illumination and man-made illumination [RHA11], because the number of used samples is so limited that their expression ability still need to be tested by other work.

4.2 Estimation of daylight spectra

Daylight includes all direct and indirect sunlight during the daytime. The spectrum of daylight is important for dealing with various imaging problems, such as color correction and color constancy in outdoor environments. According to the previous studies [JMW+64, WS82, SH98], daylight spectrum can be well approximated with a small number of basis functions. To reconstruct daylight, we need to estimate its corresponding coefficients. Here, we adopt a widely used three-basis model [WS82]:

$$l(\lambda) = \sum_{j=1}^{3} \gamma_j b_j^l(\lambda), \tag{4.1}$$

where $b_j^l(\lambda)$ is the j-th basis for daylight that is available in [WS82], and γ_j is the corresponding coefficient. Here, we show these three bases in Fig. 4.2. Recall that we used the Macbeth ColorChecker as the reference for separating the fluorescent component in Section 3.4, the appearance of its q-th patch under daylight, $(R_q, G_q, B_q)^T$ $(q = 1, ..., 24)$, can be represented as

$$R_q = \int s_q(\lambda) c_R(\lambda) l(\lambda) d\lambda. \tag{4.2}$$

Substituting Eq. (4.1) into Eq. (4.2), we obtain

$$R_q = \sum_{j=1}^{3} \gamma_j \int s_q(\lambda) c_R(\lambda) b_j^l(\lambda) d\lambda. \tag{4.3}$$

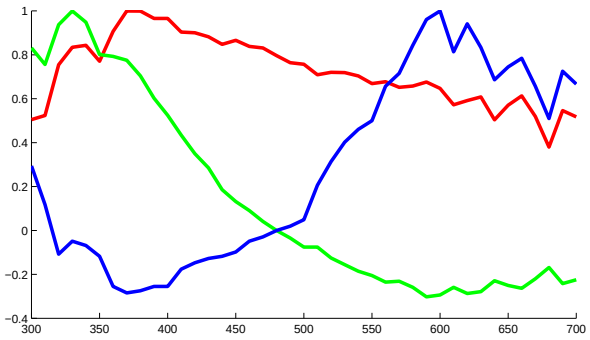

Figure 4.2: Spectral distributions of the 3 bases for daylight. Red curve: $1st$ basis; Green curve: $2nd$ basis; Blue curve: $3rd$ basis.

Three factors in the integral of Eq. (4.3) are known; only γ_j are unknown. For all 24 patches on the ColorChecker, we have 24(patch number)$\times$ 3 (channels), *i.e.*, 72, linear equations that are similar to Eq. (4.3). The three unknown coefficients γ_j can be calculated in terms of the least-squares error. With the calculated results, the spectrum of daylight can be estimated by Eq. (4.1).

The estimates for different daylight conditions are shown in Fig. 4.3. The estimated spectra are indicated by red curves, and ground truths measured by the spectrometer are indicated by black curves. We can see that they are very similar to each other. The root mean square errors (RMSE) of the estimated results are very small. Through these comparisons, we can see that the spectra of daylight can be accurately estimated by the camera spectral sensitivity,.

Based on the above discussion, it is apparent that we are capable of estimating not only camera spectral sensitivity but also the daylight spectrum from a single captured image.

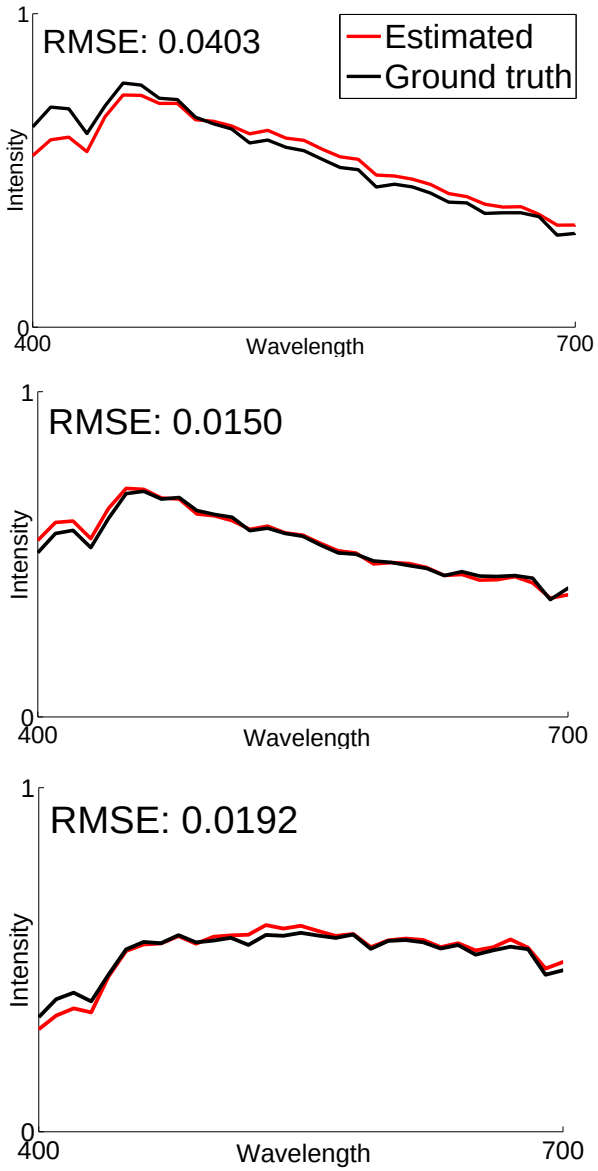

Figure 4.3: The spectral distributions of daylight can be accurately estimated from the estimated camera spectral sensitivity of a Canon 5D and the appearance of the Macbeth ColorChecker in the captured images. Upper: blue sky; Middle: cloudy sky; Lower: sun. Note that each spectrum is normalized to ensure the area of the region below the corresponding curve is a constant. Thus, the intensities are relative values for the two distributions in the same figure.

Figure 4.4: A synthetic image of a postcard composed from three real captured images. Cameras and illuminations are shown in parentheses.

4.3 Color correction

It is well known that the appearance of the same scene varies a lot under different illuminations or using different cameras. One example is shown in Fig. 4.4. This difference can be seen as multiplying albedo of scene points with different scales in the RGB channels. The scales can be calculated by multiplying the obtained camera spectral sensitivities and daylight spectra in the spectral domain, *i.e.*, $\int c_R(\lambda)l(\lambda)d\lambda$. By making use of these scales, the color of captured images under different illuminations or by different cameras can be corrected.

Let us suppose that the spectral sensitivity of a camera is $(c_R(\lambda), c_G(\lambda), c_B(\lambda))^T$, daylight is $l(\lambda)$, and the observed intensity of a scene point is $(R, G, B)^T$. For a different camera $(\overline{c_R(\lambda)}, \overline{c_G(\lambda)}, \overline{c_B(\lambda)})^T$ or under different daylight $\overline{l(\lambda)}$, the observed intensity of the same scene point is $(\overline{R}, \overline{G}, \overline{B})^T$. The relationship between these two observations can be described as

$$\overline{R} = \frac{\int \overline{c_R(\lambda)l(\lambda)}d\lambda}{\int c_R(\lambda)l(\lambda)d\lambda}R, \tag{4.4}$$

for the red channel.The relationship for the blue and green channels can be described in a similar manner.

Figure 4.5: The calibration targets are placed in the scene.

As discussed in previous sections, appearance of the fluorescent chart and the Macbeth ColorChecker is required for estimating camera spectral sensitivity and daylight spectrum. If they can be placed in the scene, a single image can capture their appearance as well as the scene (shown in Fig. 4.5). Otherwise, two images need to be taken: one of the calibration targets; another one of the scene.

Once the corresponding camera spectral sensitivity and the daylight spectra are obtained, the color of a scene's appearance can be corrected using Eq. (4.4). Here, we took images about postcards under different daylights with different cameras. These images are framed in blue in Fig. 4.6. With the estimated camera spectral sensitivities and daylight spectra, we calculated the scenes' appearances under different daylight conditions with different cameras by Eq. (4.4). The calculated results are framed in red. Each column shows a real captured image and a color corrected image captured by a different camera under different daylight conditions. We can see that, although the corrected results are not identical to the real captured images, the difference is significantly decreased, by which the effectiveness of our method can

be demonstrated.

Our method does not only work well to controlled scenes (postcards), but also can be applied to uncontrolled scenes. In Fig. 4.7, we correct the color of images about a building captured under different illuminations by different cameras. Comparing the images before and after color correction, effectiveness our method to uncontrolled scenes also can be verified.

To evaluate how well our method works on different colors, we captured two Macbeth ColorChecker images using a Canon 5D under the sun and blue sky conditions. The differences between these images before and after correction are shown in Fig. 4.8. The darker the patches are, the smaller the differences are. From the middle image, we can see that because sunlight is more reddish than light from the blue sky, for patches which have high reflectivity to red light, their differences in the red channel are obvious before color correction. After color correction, as shown in the right image, those obvious differences are greatly reduced.

Figure 4.6: The color in the captured images can be corrected to match other images captured under different illuminations or by different cameras with estimated camera spectral sensitivities and daylight spectra. Here, we show two postcard. Cameras and illuminations are shown in parentheses above.

(EPL1s,Cloudy Sky) (5D, Sun)

Figure 4.7: Color correction for a natural scene: buildings. Cameras and illuminations are shown in parentheses above.

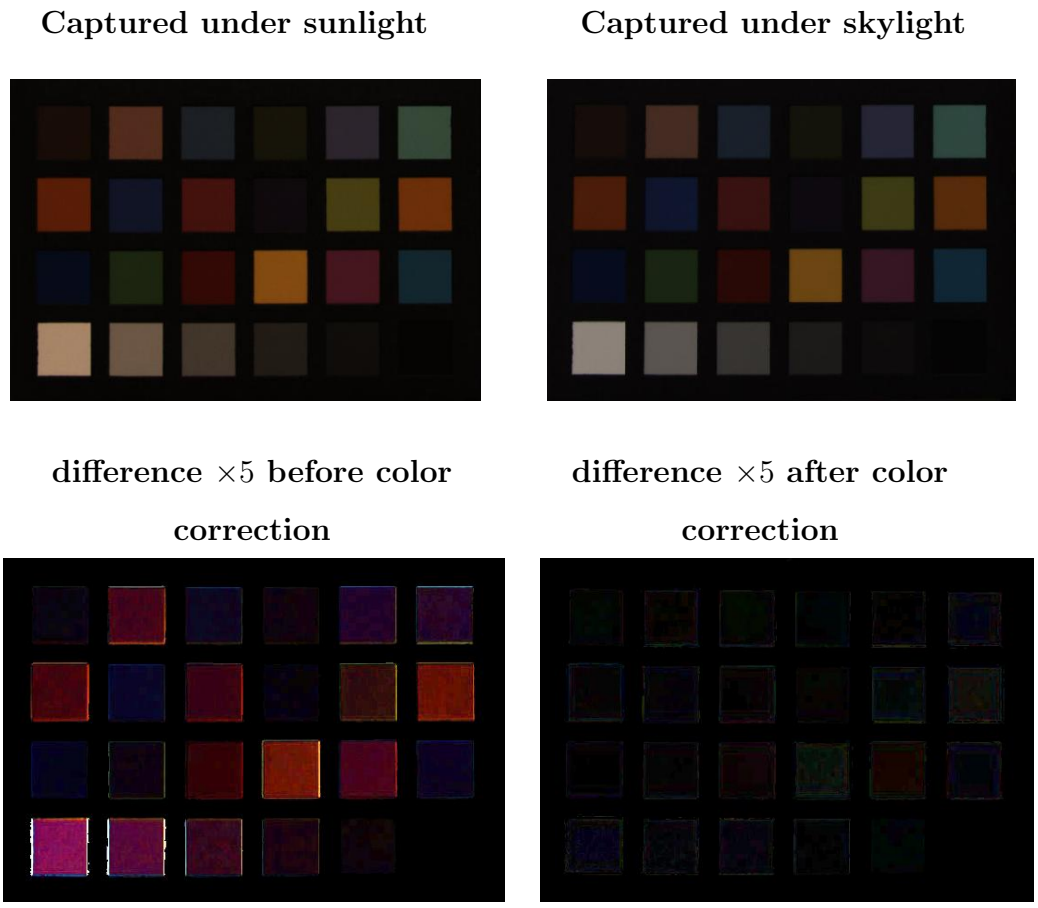

Figure 4.8: Difference between two Macbeth ColorChecker images captured under sunlight and blue sky conditions by the Canon 5D. Left: Macbeth ColorChecker; Middle: difference (×5) before correction; Right: difference (×5) after correction.

Chapter 5

Conclusions

5.1 Summary

In this thesis, we present our methods for estimating object's spectral reflectance, camera spectral sensitivity and daylight spectrum. Chapter one briefly introduces the background of this work, discusses the shortcomings of existing methods. Against these shortcomings, we propose our methods in the following chapters. In the second chapter, we build a system to recover spectral reflectance with high temporal resolution. In the system, a DLP projector has been used as the light source. With a high speed camera, scene's appearance under color-switch can be observed. Expressing spectral reflectance of objects with a 8-basis linear model, spectral reflectance of scene points can be recovered by every 5 consecutively captured images. Because the spectral measurements can be conducted at 100 Hz, our system is suitable for dynamic scene with fast-moving objects. In the third chapter, we use fluorescence to estimate camera spectral sensitivity. Under different illuminations, spectral distributions of fluorescence emitted from the same fluorescent material remains unchanged up to a scale. Using this chromatic-

ity invariance, camera spectral sensitivity can be estimated without knowing illumination spectrum. Based on the estimated camera spectral sensitivity, we reuse the images for camera spectral sensitivity estimation to estimate daylight spectra in the forth section. As a whole, the methods presented in this thesis either are easier to be carried out, or release the rigid requirement. They offer practical ways for estimating spectral information of object, cameras and illumination.

5.2 Contributions

The main contributions of this work are summarized as follow:

- Build a system with off-the-shelf components. The system is capable of conducting measurement for spectral reflectance recovery with high temporal resolution (100 Hz), enables measurement for fast-moving objects, and the recovered results are degraded little by motion blur.

- Propose a method for camera spectral sensitivity estimation without knowing illumination spectrum, which greatly releases the rigid requirement for illumination when estimating camera spectral sensitivity. Moreover, if the measurements are conducted outdoor, spectra of daylight also can be estimated without taking extra images. Color correction or color constancy of outdoor images benefit a lot from them.

5.3 Discussion

5.3.1 Linear models for spectral reflectance of objects, spectral sensitivity of cameras and spectral distributions of daylight

In this work, we use linear models to express spectral reflectance of objects, spectral sensitivity of cameras and spectral distributions of daylight. The benefits of using linear models are: (1) Dimensionality of target values can be greatly reduced. Correspondingly, number of required measurement is greatly reduced without losing accuracy. For most linear models are built by extracting principal components of datasets which contain a large number of samples, the internal correlation among samples can be well preserved by the first few basis functions. On the other hand, bases are orthogonal to each other, thus redundancy can be reduced to the minimum. Therefore, a limited number of bases can represent target value very well. For instance, spectral reflectance is a 31×1 vector. To estimate these 31 unknowns, at least 31 measurements are required. When using the linear model, 8 orthogonal bases are enough to reconstruct the spectral reflectance with good accuracy. What we need to do is estimating coefficients of these 8 bases. In this way, number of required independent measurements is reduced to 8 from 31. (2)Using linear models, number of required measurements has nothing to do with the resolution of target values. Resolution of estimated results is determined by resolution of basis functions. The number of required measurements is determined by the number of basis functions. Without using linear models, the higher the required resolution is, the more the unknowns are, the more measurements need to be conducted. Acquiring enough measurements for results with high resolution is laborious, even impossible sometimes. (3)

Simple computation. Besides linear model, there are also a lot of nonlinear models, such as Gaussian distribution, are widely used. Different from linear models, computing unknowns of the nonlinear models are always treated as optimization problems. In such a case, final results are closely related to the initial values and selected optimization methods. Global minimum or maximum can not be guaranteed. On the contrary, unknown of linear models are the coefficients of basis functions. They can be explicitly computed through Least-square error methods. Initial values are not required.

Although we can benefit a lot from using linear model, there may be no linear models for certain kinds of variables. To build linear models, there must be a few number of basis functions which are orthogonal to each other and capable of well approximating variables. For these basis functions, a dataset containing a large number of independent samples is required. These samples should be independent from each other. And, the more diverse the samples are, the higher representative the dataset is. The linear model for spectral reflectance used in this work is built on the spectral reflectance of 1257 Munsell color chips. The linear model for daylight is also built on a dataset containing 622 samples. 249 of thenm were obtained in Rochester, USA; 274 were obtained in Enfield, England; The rest 99 were obtained in Ottawa, Canada. With regard to spectral sensitivity, for there is no public datasets which contains enough samples are available, we use Fourier bases instead. Because cameras' spectral sensitivity tend to be smooth and band limited, a few number of Fourier bases are enough to provide good accuracy.

5.3.2 Using DLP projectors whose color wheels have more than 3 segments as light sources

According to [DLP], nowadays, more and more DLP projectors adopt a technique called $BrilliantColor^{TM}$ to produce more vivid images. It is a technique that uses additional color filters except for Red, Green and Blue 3 filters. There are 2 reasons for using more than 3 filters. First, expanding color gamut of the DLP projector. The color gamut of a RGB display is defined as the area of colors bounded by the triangle whose points are defined by the colorimetric settings of the red, blue, and green filters. It does not allow for the creation of vivid colors such as yellow or cyan. The reason is that these colors are outside of the area bounded by the triangle. Adding additional color filters to the rendering engine allows the projectors to expand the triangle into a wider polygon resulting in a greater selection of colors. Second, improve illumination efficiency. 3-segment color wheel does not utilize the entire energy spectrum available from the lamp inside the DLP projectors. This light loss is a result of the fact that parts of the lamp energy are not contained within the red, green, and blue filters. Using more filters which allow light in different wavelength range to get through can solve this problem.

By using DLP projectors with $BrilliantColor^{TM}$, we can get richer colors and brighter pictures. If we use such a DLP projector instead of the one we used in our system for spectral reflectance recovery, we will get more than 9 measurements which would be helpful to improve accuracy of the recovered reflectance. However, the consequent problem is that it would be hard to get the spectral distributions of the illumination bases. In case of using 3-segment color wheel projector, we are capable of getting the 3 illumination bases by inputting the projector Red (255,0,0), Green (0,255,0) and Blue (0,0,255)

respectively. Here, we take Red for instance to illustrate how DLP projectors work. To the red filter, controller inside the projector would turn DMD on to allow light getting through the filter, then emit from the projector. To green and blue filters, DMD would be turned into off state to block light from getting through them. Thus, we can get the red illumination only. However, if we use projectors equipped with more than 3 segments color wheel, we are not be able to control the switch of DMD by inputting the projectors specific values, because we have no idea how controller switch the states of the DMD to different input values. As a consequence, we will not be able to do the light decomposition to get illumination spectrum for each captured image. So, we have to decompose the DLP projectors, take out their color wheel and lamps to measure their spectral properties respectively. This would complex the calibration step significantly.

5.3.3 Suitable light source to excite fluorescence

From chapter 3, we knew that fluorescence is emission from fluorescent materials excited by light generally with higher energy. When the illumination is strong in high energy wavelength range (UV and Blue light), we can get stronger fluorescence, our method would have better accuracy. Otherwise, accuracy would be degraded by the weakness of fluorescence. So, light sources which are strong in low energy wavelength range, like halogen, are not good options for exciting fluorescence. Especially for the patches which emit blue fluorescence, because they require light with higher energy than the other patches. For daylight, we recommend using blue sky, which has comparably stronger light in high energy wavelength range, as the light source.

5.4 Future works

5.4.1 Separating photometric and geometric properties

As stated in chapter 2, we proposed a method for recovering spectral reflectance of objects' surface. The recovered results are related to not only photometric properties of objects, but also their geometric properties. In this thesis, we did not separate the effects of these two kinds of properties. In the future, we are going to use the temporal dithering caused by fast switching between "on" and "off" states ($10^6/s$) of the DMD inside DLP projectors to recover the geometric properties of objects. Then the photometric properties can be calculated easily. The biggest challenge of using temporal dithering is how to find the correspondence between the projected structured light and the captured images. For this goal, we need to design an optimized input pattern for DLP projector. About the input pattern, one requirement is that observation in consecutively captured images by the high speed camera should be significantly different from frame to frame. This enables fast and accurate matching between projected light and observation. Another requirement is that the pattern should be bright, which would be helpful to avoid the degradation of recovered results caused by noise.

5.4.2 Spectral reflectance recovery for non-opaque objects

In chapter 2, we restrict objects to opaque objects. In real world, there are a lot of transparent as well as translucent objects. Their appearance is related to not only reflection but also sophisticated refection, interreflection,

subsurface scattering *etc.* To separate effects of these phenomenons, the best approach is modeling how light transports in scenes. Recently, a lot of works have been published on light transport [YDMH99, JMLH01, SCG+05, MYR10, GTNZ09]. However, these detailed analysis about light transport requires taking a large set of images, the whole process is time-consuming. For spectral reflectance, we need the direct reflectance component only. To separate direct and global components in captured images of a scene, Nayar *et al* proposed a method by using spatially high frequency illumination [NKGR06]. Using the separated direct component as the observation, spectral reflection of non-opaque objects can be correctly computed by our method. How to incorporate the high frequency illumination properly will be the key problem to be solved.

5.4.3 Optimized fluorescent chart for camera spectral sensitivity estimation

To estimate camera spectral sensitivity, we built a fluorescent chart by using a set of fluorescent paint in chapter 3. In section 3.6.1, we mentioned that estimated spectral sensitivity of the blue channel deviate more than green and red channels, and that accuracy of estimated results under sunlight is not as good as those under skylight or fluorescent lamp. Our explanation is that although fluorescence emitted from the same fluorescent patch under different illuminations remains the same up to a certain scale, intensities of emitted fluorescence are illumination-dependent. This intensity variation results in the accuracy variation. If we can optimize the selection of paint for camera spectral sensitivity estimation, it may be possible to avoid the accuracy variation. However, optimal fluorescent paint selection is a difficult task. The main reason is that there is no publicly available dataset about

paint which contains the emission spectra of a large set of fluorescent paint. We tried several sets of fluorescent paint produced by different manufactures, but it is often observed that different kinds of paint have the same emission spectra or some emission spectra are linearly dependent. This may result from those paint shares the same fluorescent ingredients. Therefore, we plan to pay our attention to a wider range of fluorescent materials besides paint.

Fluorescence has been well studied in medical and biological fields. A lot of fluorescent dyes are used as cell and tissue labels, their emission spectra are already available in [Flu]. Based on this set, we hope it is possible to design an optimized fluorescent chart by which the same level of accuracy for camera spectral sensitivity estimation can be guaranteed under different illuminations.

5.4.4 Illumination estimation using absorption spectra of different fluorescent materials

Color values have 2 independent properties: chromaticity and intensity. In chapter 3, we use the chromaticity invariance of fluorescent to estimate camera spectral sensitivity under unknown illumination. Although chromaticity of fluorescence is independent from illuminations, intensities of the fluorescence are tightly related to illumination spectra. Recall Eq. (3.1), intensity of fluorescence depends on the absorption spectrum of fluorescent material and the spectrum of illumination. Once its absorption spectrum is calibrated, intensity of illumination in the wavelength range of its absorption spectrum can be estimated by the intensity of corresponding fluorescence. Using a number of different fluorescent materials with different absorption spectra, illumination in the visible wavelength can be computed from the intensities of the fluorescence from them.

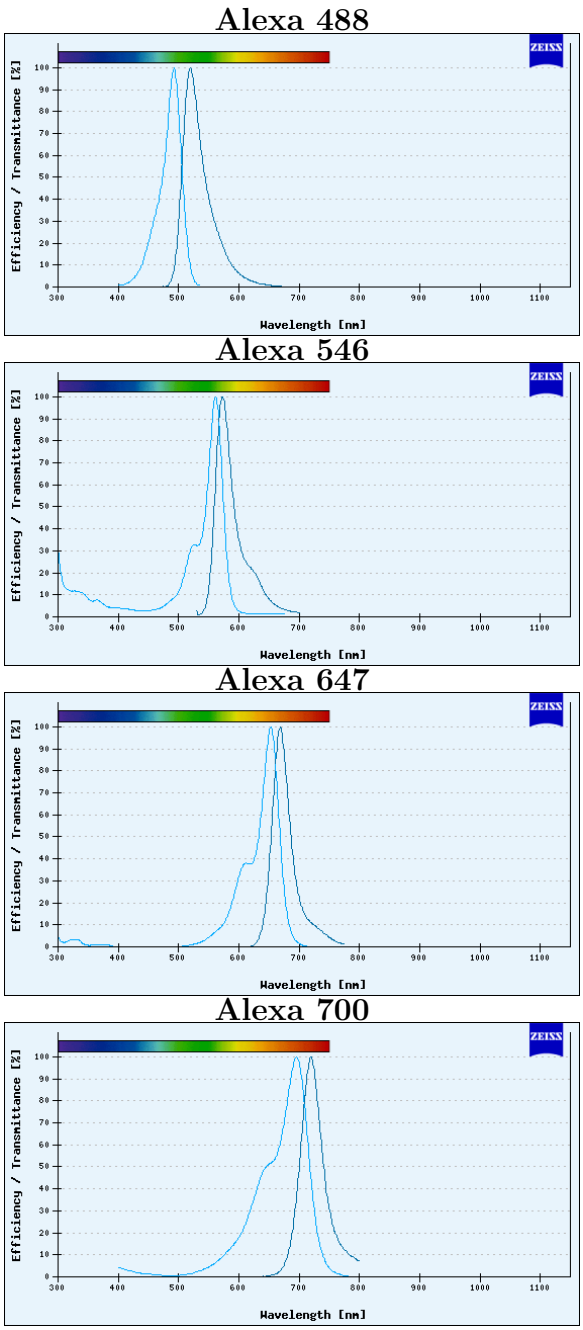

Figure 5.1: Absorption and emission spectra of 4 fluorescent dyes in Alex Fluor family. The absorption spectra are indicated by light blue; the emission spectra are indicated by dark blue.

The advantages of using intensity variation of fluorescence to estimate illumination are (1) Dimensionality of illumination is not limited to the dimensionality of reflectance. (2) Estimation of camera spectral sensitivity and illumination spectrum can be done simultaneously by just taking a single image. The difficulty of using this method is how to acquire the expected collection of fluorescent materials. Applying genetic algorithm to a dataset containing a large number of fluorescent materials may solve this problem. Such a dataset is available in [Car], Fig. 5.1 shows us the absorption and emission spectra of 4 different kinds of fluorescent materials in them.

Bibliography

[AACP99] A. Abrardo, L. Alparone, I. Cappellini, and A. Prosperi. constancy from multispectral images. In *Proc. IEEE International Conference Computer Vision*, volume 3, pages 570–574, 1999.

[AAWB09] Xiaobai Sun Ashwin A. Wagadarikar, Nikos P. Pitsianis and David J. Brady. Video rate spectral imaging using a coded aperture snapshot spectral imager. *Optics Express*, 17(8):6368–6388, 2009.

[Ass10] European Machine Vision Association. Methods for spectral sensitivity. *EMVA Standard 1288:Standard for Characterization of Image Sensors and Cameras*, page 28, 2010.

[AWB08] Rebecca Willett Ashwin Wagadarikar, Renu John and David Brady. Single disperser design for coded aperture snapshot spectral imaging. *Applied Optics*, 47(10):B44–B51, 2008.

[Bar99] K. Barnard. Color constancy with fluorescent and surfaces. In *Proc. IS&T/SID Color Imaging Conference*, pages 257–261, 1999.

[BF02] K. Barnard and B. Funt. Camera characterization for color research. *COLOR research and application*, 27:152–163, June 2002.

[BG06] D. J. Brady and M. E. Gehm. Compressive imaging spectrometers using coded apertures. volume 6246, 2006.

[Car] https://www.micro-shop.zeiss.com/?s=2525647761b33&l=en&p=us&f=f.

[CCO00] Chuan-Chin Chiao, Thomas W. Cronin, and Daniel Osorio. Color signals in natural scenes: characteristics of reflectance spectra and effects of natural illuminants. *Journal of the Optical Society of America A*, 17(2):218–224, 2000.

[CHM10] Chi Cui, Yoo Hyunjin, and Ben-Ezra Moshe. Multi-spectral imaging by optimized wide band illumination. *International Journal on Computer Vision*, 86:140–151, Jan 2010.

[Dan92] James L. Dannemiller. Spectral reflectance of natural objects: how many basis functions are necessary? *Journal of the Optical Society of America A*, 9(4):507–515, 1992.

[DD95] Michael Descour and Eustace Dereniak. Computed-tomography imaging spectrometer: experimental calibration and reconstruction results. *Applied Optics*, 34(22):4817–4826, 1995.

[DLP] http://www.dlp.com/projector/dlp-innovations/brilliantcolor.aspx.

[Don54] R. Donaldson. Spectrophotometry of fluorescent pigments. *British Journal of Applied Physics*, pages 210–214, 1954.

[DTCL09] Hao Du, Xin Tong, Xun Cao, and Stephen Lin. A prism-based system for multispectral video acquisition. In *Proc. IEEE International Conference Computer Vision*, Oct 2009.

[DVD+97] Michael R. Descour, Curtis E. Volin, Eustace L. Dereniak, Tim M. Gleeson, Mark F. Hopkins, Daniel W. Wilson, and Paul D. Maker. Demonstration of a computed-tomography imaging spectrometer using a computer-generated hologram disperser. *Applied Optics*, 36(16):3694–3698, 1997.

[DXW00] Jeffrey M. DiCarlo, Feng Xiao, and Brian A Wandell. Illuminating illumination. In *Proc. Ninth Color Imaging Conference*, pages 27–34, 2000.

[DXW03] Jeffrey M. DiCarlo, Feng Xiao, and Brian A Wandell. Spectral estimation theory: beyond linear but before bayesian. *Journal of the Optical Society of America A*, 20(7):1261–1270, 2003.

[D'Z92] Michael D'Zmura. Color constancy: surface color from changing illumination. *Journal of the Optical Society of America A*, 9(3):490–493, 1992.

[Ebn07] M. Ebner. Estimating the spectral sensitivity of a digital sensor using calibration targets. In *Proc. Conference on Genetic and Evolutionary Computation*, pages 642–649, 2007.

[FHH98] G. D. Finlayson, S. D. Hordley, and P. Hubel. Characterization of scanner sensitivity. In *Proc. Color Imaging Conference*, pages 90–95, 1998.

[FHH01] Graham Finlayson, Steven Hordley, and Paul Hubel. Color by correlation: A simple, unifying framework for color constancy.

Pattern Analysis and Machine Intelligence , IEEE Transactions on, 23(11):1209–1221, 2001.

[Fin95] G. D. Finlayson. Phd thesis: Coefficient color constancy. *Simon Fraser University*, 1995.

[Flu] http://www.mcb.arizona.edu/ipc/fret/index.html.

[For90] D. Forsyth. A novel algorithm for color constancy. *International Journal on Computer Vision*, 5(1):5–36, 1990.

[Gat00a] Nahum Gat. Imaging spectroscopy using tunable filters : A review. In *Proc. SPIE 4056*, volume 4056, pages 50–64, April 2000.

[Gat00b] Nahum Gat. Imaging spectroscopy using tunable filters: A review. In *Proc. SPIE Conf. Wavelet Appl. VII*, volume 4056, pages 50–64, 2000.

[GOL49] MARCEL T. E. GOLAY. Multi-slit spectrometry. *Journal of the Optical Society of America A*, 39(6):437–444, 1949.

[GTNZ09] Mohit Gupta, Yuandong Tian, Srinivasa G. Narasimhan, and Li Zhang. (de) focusing on global light transport for active scene recovery. In *Proc. IEEE Conference on Computer Vision and Pattern Recognition*, 2009.

[HD08] Nathan Hagen and Eustace L. Dereniak. Analysis of computed tomographic imaging spectrometers. i. spatial and spectral resolution. *Applied Optics*, 47(28):85–95, 2008.

[HDS06] Nathan Hagen, Eustace L. Dereniak, and David T. Sass. Maximizing the resolution of a ctis instrument. volume 6302, 2006.

[HFHG+05] Andrew R. Harvey, David W. Fletcher-Holmes, Alistair Gorman, Kirsten Altenbach, Jochen Arlt, and Nick D Read. Spectral imaging in a snapshot. In *Proc. SPIE*, volume 5694, 2005.

[HFI+08] Matthias Hullin, Martin Fuchs, Ivo Ihrke, Hans-Peter Seidel, and Hendrik Lensch. Fluorescent immersion range scanning. In *Proc. SIGGRAPH*, 2008.

[HHA+10] Matthias Hullin, Johannes Hanika, Boris Ajdin, Hans-Peter Seidel, Jan Kautz, and Hendrik Lensch. Acquisition and analysis of bispectral bidirectional reflectance and reradiation distribution functions. In *Proc. SIGGRAPH*, 2010.

[HOH+94] Esko Herrala, Jukka T. Okkonen, Timo S. Hyvarinen, Mauri Aikio, and Jorma Lammasniemi. Imaging spectrometer for process industry applications. In *Proc. SPIE*, volume 2248, pages 33–40, 1994.

[HRMT94] Clifford C. Hoyt Hannah R. Morris and Patrick J. Treado. Imaging spectrometers for fluorescence and raman microscopy: Acousto-optic and liquid crystal tunable filters. 48(7):857–866, 1994.

[HVJ00] Q. S. Hanley, P. J. Verveer, and T. M. Jovin. Three-dimensional spectral imaging by hadamard transform spectroscopy in a programmable array microscope. *Journal of Microscopy*, 197:5–14, 2000.

[Jas96] M. Jasinski. Estimation of subpixel vegetation density of natural regions using satellite multispectral imagery. *Geoscience and Remote Sensing, IEEE Transactions on*, 34:804–813, May 1996.

[J.C64] J.Cohen. Dependency of the spectral reflectance curves of the munsell color chips. *Psychon. Sci*, 1:369–370, 1964.

[JF99] G. Johnson and M. Fairchild. Full-spectral color calculations in realistic image synthesis. *IEEE Computer Graphics and Applications*, 19:47–53, Jul/Aug 1999.

[JMLH01] Henrik Wann Jensen, Steve Marschner, Marc Levoy, and Pat Hanrahan. A practical model for subsurface light transport. In *Proc. SIGGRAPH*, 2001.

[JMMB97] Myoung An Jonathan M. Mooney, Virgil E. Vickers and Andrzej K. Brodzik. High-throughput hyperspectral infrared camera. *Journal of the Optical Society of America A*, 14(11):2951–2961, 1997.

[JMW+64] Deane Judd, David Macadam, Gutnter Wyszecki, H. Budde, H. Condit, S. Henderson, and J. Simonds. Spectral distribution of typical daylight as a function of correlated color temperature. *Journal of the Optical Society of America A*, 54(8):1031–1036, 1964.

[KN07] Kiyosumi Kidono and Yoshiki Ninomiya. Visibility estimation under night-time conditions using a multiband camera. In *Proc. IEEE Intelligent Vehicles Symposium*, pages 1013–1018, 2007.

[KPJ06] Oili Kohonen, Jussi Parkkinen, and Timo Jaaskelainen. Databases for spectral color science. *Color Research And Application*, 31(5):381–390, 2006.

[LPL+05] Zhenyu Li, Demetri Psaltis, Wenhai Liu, William R. Johnson, and Gregory Bearman. Volume holographic spectral imaging. In *Proc. SPIE*, volume 5694, 2005.

[Mac] http://www.babelcolor.com/main_level/ColorChecker.htm.

[Mal86] Laurence T. Maloney. Evaluation of linear models of surface spectral reflectance with small numbers of parameters. *Journal of the Optical Society of America A*, 3(10):1673–1683, 1986.

[MAR11] Rump Martin, Zinke Arno, and Klein Reinhard. Practical spectral characterization of trichromatic cameras. In *Proc. SIGGRAPH ASIA*, December 2011.

[MEGS07] D. J. Brady R. M. Willett M. E. Gehm, R. John and T. J. Schulz. Single-shot compressive spectral imaging with a dual-disperser architecture. *Optics Express*, 15(21):14013–14027, 2007.

[MPW06] Christian Munzenmayer, Dietrich Paulus, and Thomas Wittenberg. A spectral color correction framework for medical applications. *Biomedical Engineering, IEEE Transactions on*, 53(2):254–265, 2006.

[MRT08] Ankit Mohan, Ramesh Raskar, and Jack Tumblin. Agile spectrum imaging: Programmable wavelength modulation for cameras and projectors. In *Proc. Eurographics*, volume 27, pages 709–717, 2008.

[MW86] Laurence T. Maloney and Brain A. Wandell. Color constancy: a method for recovering surface spectral reflectance. *Journal of the Optical Society of America A*, 3(1):29–33, 1986.

[MYR10] Yasuhiro Mukaigawa, Yasushi Yagi, and Ramesh Raskar. Analysis of light transport in scattering media. In *Proc. IEEE Conference on Computer Vision and Pattern Recognition*, 2010.

[NBB06] Shree K. Nayar, Vlad Branzoi, and Terry. E. Boult. Programmable imaging: Towards a flexible camera. *International Journal on Computer Vision*, 70:7–22, Oct 2006.

[NKGR06] Shree K. Nayar, Gurunandan Krishnan, Michael D. Grossberg, and Ramesh Raskar. Fast separation of direct and global components of a scene using high frequency illumination. In *Proc. SIGGRAPH*, 2006.

[NKY08] Srinivasa G. Narasimhan, Sanjeev J. Koppal, and Shuntaro Yamazaki. Temporal dithering of illumination for fast active vision. In *Proc.European Conference Computer Vision*, Oct 2008.

[PHJ89] J. P. S. Parkkinen, J. Hallikainen, and T. Jaaskelainen. Characteristic spectra of munsell colors. *Journal of the Optical Society of America A*, 6(2):318–322, 1989.

[PLGN07] Jong-Il Park, Moon-Hyun Lee, Michael D. Grossberg, and Shree K. Nayar. Multispectral Imaging Using Multiplexed Illumination. In *Proc.IEEE International Conference Computer Vision*, Oct 2007.

[RHA11] Sivalogeswaran Ratnasingam and Javier Hernandez-Andres. Illuminant spectrum estimation at a pixel. *Journal of the Optical Society of America A*, 28(4):696–703, 2011.

[RJ99] Mitchell R. Rosen and Xiao-Yun (Willie) Jiang. Lippmann2000: A spectral image database under construction. In *Proc. Inter-*

national Symposium on Multispectral Imaging and Color Reproduction for Digital Archives, pages 117–122, 1999.

[ROGW98] Charles M. Sarture Thomas G. Chrien Mikael Aronsson Bruce J. Chippendale Jessica A. Faust Betina E. Pavri Christopher J. Chovit Manuel Solis Martin R. Olah Robert O. Green, Michael L. Eastwood and Orlesa Williams. Imaging spectroscopy and the airborne visible/infrared imaging spectrometer (aviris). 65:224–248, 1998.

[SBMS93] R. L. Rairden S. B. Mende, E. S. Claflin and G. R. Swenson. Hadamard spectroscopy with a two-dimensional detecting array. *Applied Optics*, 32(34):7095–7105, 1993.

[SCG+05] Pradeep Sen, Billy Chen, Gaurav Garg, Stephen R. Marschner, Mark Horowitz, Marc Levoy, and Hendrik P. A. Lensch. Dual photography. In *Proc. SIGGRAPH*, 2005.

[Sen] http://www.cvl.iis.u-tokyo.ac.jp/~zhao/database.html.

[SH98] David Slater and Glenn Healey. What is the spectral dimensionality of illumination functions in outdoor scenes? In *Proc. IEEE Conference on Computer Vision and Pattern Recognition*, 1998.

[SH99] David Slater and Glenn Healey. Material classification for 3d objects in aerial hyspectral images. In *Proc. IEEE Conference on Computer Vision and Pattern Recognition*, volume 2, pages 268–273, 1999.

[SN02] Yoav Y. Schechner and Shree K. Nayar. Generalized mosaicing: Wide field of view multispectral imaging. *Pattern Analysis and Machine Intelligence, IEEE Transactions on*, 24(10):1334–1348, 2002.

[TB06] Di-Yuan Tzeng and Roy S. Berns. A review of principal component analysis and its applications to color technology. *Color Research And Application*, 30(2):84–98, 2006.

[Tom96] Shoji Tominaga. Multichannel vision system for estimating surface and illumination functions. *Journal of the Optical Society of America A*, 13(11):2163–2173, 1996.

[TOY93] Akinori Takahashi Takayuki Okamoto and Ichirou Yamaguchi. Simultaneous acquisition of spectral and spatial intensity distribution. *Applied Spectroscopy*, 47(8):1198–1202, 1993.

[TW01] M. Thomson and S. Westland. Colour-imager characterization by parametric fitting of sensor responses. *COLOR research and application*, 26:442–449, December 2001.

[UDHS10] P. Urban, M. Desch, K. Happel, and D. Spiehl. Recovering camera sensitivities using target-based reflectances captured under multiple led-illuminations. In *Proc. Workshop on Color Image Processing*, pages 9–16, 2010.

[VMHD07] Corrie Vandervlugta, Hugh Mastersonb, Nathan Hagena, and Eustace L. Dereniaka. Reconfigurable liquid crystal dispersing element for a computed tomography imaging spectrometer. volume 6565, 2007.

[WFHH05] David William, Fletcher-Holmes, and Andrew Robert Harvey. Real-time imaging with a hyperspectral fovea. *Journal of the Optical Society of America A*, 7(6):298–302, 2005.

[WHD03] A. Wenger, T. Hawkins, and P. Debevec. Optimizing color matching in a lighting reproduction system for complex subject and illuminant spectra. In *Proc. 14th Eurographics workshop on Rendering*, 2003.

[WLP04] George Barbastathis Wenhai Liu and Demetri Psaltis. Volume holographic hyperspectral imaging. 43(18):3581–3599, 2004.

[WRJB06] Daniel W. Wilson William R. Johnson and Greg Bearman. Spatial-spectral modulating snapshot hyperspectral imager. *Applied Optics*, 45(9):1898–1908, 2006.

[WS82] G. Wyszecki and W. Stiles. Color science: Concepts and methods, quantitative data and formulae. *Wiley-Interscience publication*, 1982.

[YDMH99] Yizhou Yu, Paul Debevec, Jitendra Malik, and Tim Hawkins. Inverse global illumination: Recovering reflectance models of real scenes from photographs. In *Proc. SIGGRAPH*, 1999.

[YHF06a] M. Yamaguchi, H. Haneishi, and H. Fukuda. High-fidelity video and still-image communication based on spectral information: Natural vision system and its applications. In *Proc. SPIE 6062*, volume 6062, 2006.

[YHF+06b] Masahiro Yamaguchi, Hideaki Haneishi, Hiroyuki Fukuda, Junko Kishimoto, Hiroshi Kanazawa, Masaru Tsuchida, Ryo

Iwama, and Nagaaki Ohyama. High-fidelity video and still-image communication based on spectral information: Natural vision system and its applications. In *Proc. SPIE-IST Electronic Imaging*, volume 6062, 2006.

[ZH04] Song Zhang and Peisen Huang. High-resolution, real-time 3d shape acquisition. In *Proc. IEEE Conference on Computer Vision and Pattern Recognition Workshops*, volume 3, pages 28–37, 2004.

[ZS11] Cherry Zhang and Imari Sato. Separating reflective and fluorescent components of an image. In *Proc. IEEE Conference on Computer Vision and Pattern Recognition*, 2011.